



**NAVAL
POSTGRADUATE
SCHOOL**

MONTEREY, CALIFORNIA

THESIS

**WIND TURBINE RADAR INTERFERENCE
REDUCTION USING SHROUD AND SCREENS**

by

Chai Meng Lim

March 2018

Thesis Advisor:
Second Reader:

David C. Jenn
Terry E. Smith

Approved for public release. Distribution is unlimited.

THIS PAGE INTENTIONALLY LEFT BLANK

REPORT DOCUMENTATION PAGE			Form Approved OMB No. 0704-0188	
Public reporting burden for this collection of information is estimated to average 1 hour per response, including the time for reviewing instruction, searching existing data sources, gathering and maintaining the data needed, and completing and reviewing the collection of information. Send comments regarding this burden estimate or any other aspect of this collection of information, including suggestions for reducing this burden, to Washington headquarters Services, Directorate for Information Operations and Reports, 1215 Jefferson Davis Highway, Suite 1204, Arlington, VA 22202-4302, and to the Office of Management and Budget, Paperwork Reduction Project (0704-0188) Washington DC 20503.				
1. AGENCY USE ONLY (Leave blank)	2. REPORT DATE March 2018	3. REPORT TYPE AND DATES COVERED Master's thesis		
4. TITLE AND SUBTITLE WIND TURBINE RADAR INTERFERENCE REDUCTION USING SHROUD AND SCREENS			5. FUNDING NUMBERS	
6. AUTHOR(S) Chai Meng Lim				
7. PERFORMING ORGANIZATION NAME(S) AND ADDRESS(ES) Naval Postgraduate School Monterey, CA 93943-5000			8. PERFORMING ORGANIZATION REPORT NUMBER	
9. SPONSORING / MONITORING AGENCY NAME(S) AND ADDRESS(ES) N/A			10. SPONSORING / MONITORING AGENCY REPORT NUMBER	
11. SUPPLEMENTARY NOTES The views expressed in this thesis are those of the author and do not reflect the official policy or position of the Department of Defense or the U.S. Government. IRB number ___N/A___.				
12a. DISTRIBUTION / AVAILABILITY STATEMENT Approved for public release. Distribution is unlimited.			12b. DISTRIBUTION CODE	
13. ABSTRACT (maximum 200 words) The benefits of wind turbines as a means for renewable energy generation are offset by the turbines' creation of signal interference, such as Doppler shift, for radar systems used for air traffic control and weather forecasting. This restricts the placement of wind farms in the vicinity of radar installations. In this research, we investigate the effectiveness of placing a screen in front of a wind turbine in reducing turbine-generated Doppler shift interference. Software-defined radar (SDR) transmitting in continuous-wave mode was used to collect data required to analyze the signature of the Doppler returns. We built a rotator (i.e., an arm with metallic ball attached to one end) to establish the computation method to analyze the Doppler signature. Once the computation method was determined, measurements at various angles were carried out on the rotator with the aluminum shroud and screen included. Similar measurements were carried out on the scaled-down wind turbine model in Port Hueneme, CA, for comparison. This research shows that the SDR can be used to accurately measure the Doppler shift, and high-quality screens are effective in reducing the turbine-generated Doppler shift by more than 20 dB.				
14. SUBJECT TERMS wind turbine, wind farm, radar, Doppler interference, shrouds, screens			15. NUMBER OF PAGES 73	
			16. PRICE CODE	
17. SECURITY CLASSIFICATION OF REPORT Unclassified	18. SECURITY CLASSIFICATION OF THIS PAGE Unclassified	19. SECURITY CLASSIFICATION OF ABSTRACT Unclassified	20. LIMITATION OF ABSTRACT UU	

THIS PAGE INTENTIONALLY LEFT BLANK

Approved for public release. Distribution is unlimited.

**WIND TURBINE RADAR INTERFERENCE REDUCTION USING SHROUD
AND SCREENS**

Chai Meng Lim
Military Expert 5, Republic of Singapore Navy
B.Eng., National University of Singapore, 2011

Submitted in partial fulfillment of the
requirements for the degree of

MASTER OF SCIENCE IN ELECTRICAL ENGINEERING

from the

**NAVAL POSTGRADUATE SCHOOL
March 2018**

Approved by: David C. Jenn
Thesis Advisor

Terry E. Smith
Second Reader

R. Clark Robertson
Chair, Department of Electrical and Computer Engineering

THIS PAGE INTENTIONALLY LEFT BLANK

ABSTRACT

The benefits of wind turbines as a means for renewable energy generation are offset by the turbines' creation of signal interference, such as Doppler shift, for radar systems used for air traffic control and weather forecasting. This restricts the placement of wind farms in the vicinity of radar installations. In this research, we investigate the effectiveness of placing a screen in front of a wind turbine in reducing turbine-generated Doppler shift interference. Software-defined radar (SDR) transmitting in continuous-wave mode was used to collect data required to analyze the signature of the Doppler returns. We built a rotator (i.e., an arm with metallic ball attached to one end) to establish the computation method to analyze the Doppler signature. Once the computation method was determined, measurements at various angles were carried out on the rotator with the aluminum shroud and screen included. Similar measurements were carried out on the scaled-down wind turbine model in Port Hueneme, CA, for comparison. This research shows that the SDR can be used to accurately measure the Doppler shift, and high-quality screens are effective in reducing the turbine-generated Doppler shift by more than 20 dB.

THIS PAGE INTENTIONALLY LEFT BLANK

TABLE OF CONTENTS

I.	INTRODUCTION.....	1
A.	OVERVIEW.....	1
B.	RADAR INTERFERENCE FROM WIND FARMS.....	2
C.	MITIGATION APPROACHES	3
1.	Siting Options.....	3
2.	Radar Options.....	3
3.	Wind Turbine Options	4
D.	INTERFERENCE REDUCTION TECHNIQUES.....	4
1.	RCS Reduction for Tower and Blades.....	4
2.	Addition of Shroud and Wire Grid Screen.....	5
E.	RELATED WORKS.....	6
F.	THESIS OBJECTIVES.....	6
G.	THESIS OUTLINE.....	7
II.	CW RADAR OPERATION AND WT RCS.....	9
A.	CW RADAR OPERATION.....	9
B.	INTERFERENCE FROM WIND TURBINES.....	10
1.	Radar Cross Section of the Wind Turbine	10
2.	Doppler Frequency Shift from the Wind Turbine.....	11
C.	SYSTEM DESCRIPTION AND SIGNAL PROCESSING	11
1.	Software-Defined Radar.....	11
2.	Extracting Doppler Frequency Shift.....	13
3.	Time-Frequency Analysis of Doppler Signature.....	14
III.	SIMULATION AND MEASUREMENT RESULTS	19
A.	SIMULATION AND MEASUREMENT FOR THE SCREEN	19
1.	Simulation Result for Screen with 0.5 Inch by 0.5 Inch Opening.....	20
2.	Simulation Result for Wire Mesh.....	20
3.	Insertion Loss Measurement for Wire Mesh.....	21
B.	RADAR MEASUREMENT RESULTS.....	23
1.	Measurement Setup Using SDR	23
2.	Measurement Results for Metallic Ball on Rotating Arm	26
3.	Measurement Results for the Wind Turbine Model.....	38
IV.	SUMMARY AND CONCLUSIONS	51
A.	SUMMARY OF FINDINGS	51

1.	Findings for Rotator	51
2.	Findings for Wind Shroud Model	52
B.	FUTURE WORK	52
LIST OF REFERENCES		53
INITIAL DISTRIBUTION LIST		55

LIST OF FIGURES

Figure 1.	Wind Power Installation Capacity from 1999 to 2016. Source: [3].	1
Figure 2.	Doppler Returns from Wind Farms (yellow circle) on the Weather Radar Display. Source: [5].	2
Figure 3.	Data Fusion Architecture. Source: [6].	4
Figure 4.	Shroud Model Used to Investigate Wind Capturing Efficiency. Source: [8].	5
Figure 5.	Simple CW Radar Block Diagram. Source: [13].	9
Figure 6.	Doppler Shifts Extracted by a Quadrature Detector. Source: [12].	10
Figure 7.	SDR System Block Diagram. Source: [16].	12
Figure 8.	Short-Time Fourier Transform. Source: [19].	15
Figure 9.	Time/Frequency Uncertainty of a Rectangular Window. Source: [19].	15
Figure 10.	Best Time/Frequency Resolution with Gaussian Window. Source: [19].	16
Figure 11.	Estimating Insertion Loss of Plane Wave Passing through Screens: (a) Simulation of Screen Using Floquet Technique (unit cell highlighted). (b) Photograph of Actual Screen	19
Figure 12.	S11 Parameters for Screen with Opening of 0.5 Inches by 0.5 Inches	20
Figure 13.	S11 Parameters for Mesh of 1.0 mm by 1.0 mm Opening	21
Figure 14.	Wire Mesh of 1.0 mm by 1.0 mm Openings	21
Figure 15.	Baseline Measurement Using Labvolt Instrumentation	22
Figure 16.	Measurement with Wire Mesh Using Labvolt Instrumentation	22
Figure 17.	Equipment Setup to Determine Measurement Accuracy of SDR	23
Figure 18.	Received Signal in dB Versus Time with No Attenuation Applied: (a) Spectrogram and (b) Power	24

Figure 19.	Received Signal in dB Versus Time with 10 dB Attenuation Applied: (a) Spectrogram and (b) Power	24
Figure 20.	Received Signal in dB Versus Time with 20 dB Attenuation Applied: (a) Spectrogram and (b) Power	25
Figure 21.	Received Signal in dB Versus Time with 30 dB Attenuation Applied: (a) Spectrogram and (b) Power	25
Figure 22.	Measurement at 0° Offset Angle	27
Figure 23.	Measurement at 60° Offset Angle	28
Figure 24.	Doppler Spectrogram (dB) for Antenna at: (a) 0°, (b) 20°, (c) 40°, and (d) 60° Offset Angle from Rotator at 80 rpm.....	29
Figure 25.	Comparison of the Values between Theoretical Doppler and Measured Doppler Frequencies for Rotator.....	30
Figure 26.	Power Plot for Antenna at (a) 0°, (b) 20°, (c) 40°, and (d) 60° Offset Angle from Rotator at 80 rpm.....	31
Figure 27.	Different Configurations for Measurements: (a) Shroud, (b) Shroud and 0.5 Inch by 0.5 Inch Screen, and (c) Shroud and 1.0 mm by 1.0 mm Wire Mesh	32
Figure 28.	Side View of the Setup for Wind Turbine Measurement	38
Figure 29.	Top View of the Setup for Wind Turbine Measurement	38
Figure 30.	Wind Turbine Model Configurations: (a) Bare, (b) with Shroud, and (c) Shroud and 0.5 Inch by 0.5 Inch Screen.....	39
Figure 31.	Doppler Spectrogram for Antenna at 90° Offset Angle from Wind Turbine Model at 120 rpm	40
Figure 32.	Doppler Spectrogram for Antenna at (a) 0°, (b) 20°, (c) 40°, and (d) 60° Offset Angle from Wind Turbine Model at 120 rpm	41
Figure 33.	Comparison between Theoretical Doppler and Measured Doppler Frequencies for Wind Turbine Model.....	42
Figure 34.	Power Plot for Antenna at (a) 0°, (b) 20°, (c) 40°, and (d) 60° Offset Angle from Wind Turbine Model at 120 rpm.....	43

LIST OF TABLES

Table 1.	SDR-KIT 980AD Parameters. Source: [16].	13
Table 2.	Result Summary for Different Attenuation Applied	26
Table 3.	Comparison between Theoretical and Measured Doppler Frequencies	29
Table 4.	Spectrogram and Power Plot Comparison for Antenna at 0° Offset Angle for Different Cases for Rotator	34
Table 5.	Spectrogram and Power Plot Comparison for Antenna at 20° Offset Angle for Different Cases for Rotator	35
Table 6.	Spectrogram and Power Plot Comparison for Antenna at 40° Offset Angle for Different Cases for Rotator	36
Table 7.	Spectrogram and Power Plot Comparison for Antenna at 60° Offset Angle for Different Cases for Rotator	37
Table 8.	Comparison between Theoretical and Measured Doppler Return Frequency for Wind Turbine Model	42
Table 9.	Spectrogram and Power Plot Comparison for Antenna at 0° Offset Angle for Different Cases for Wind Turbine Model	45
Table 10.	Spectrogram and Power Plot Comparison for Antenna at 20° Offset Angle for Different Cases for Wind Turbine Model	46
Table 11.	Spectrogram and Power Plot Comparison for Antenna at 40° Offset Angle for Different Cases for Wind Turbine Model	47
Table 12.	Spectrogram and Power Plot Comparison for Antenna at 60° Offset Angle for Different Cases for Wind Turbine Model	48

THIS PAGE INTENTIONALLY LEFT BLANK

LIST OF ACRONYMS AND ABBREVIATIONS

ADC	Analog-to-Digital Converter
CST	Computer Simulation Technology
CW	Continuous Wave
DAC	Digital-Analog Converter
DC	Direct Current
FMCW	Frequency-Modulated Continuous Wave
FPGA	Field-Programmable Gate Array
FSK	Frequency-Shift Keying
FT	Fourier Transform
GUI	Graphical User Interface
I	In-phase
MWS	Microwave Studio
Q	Quadrature
RAM	Radar Absorbent Material
RCS	Radar-Cross Section
RF	Radio Frequency
RLOS	Radar Line-of-Sight
SDR	Software-Defined Radar
STFT	Short Time Fourier Transform
TX	Transmit
USB	Universal Serial Bus
VCO	Voltage-Controlled Oscillator
WT	Wind Turbine

THIS PAGE INTENTIONALLY LEFT BLANK

ACKNOWLEDGMENTS

I would like to thank my advisor, Professor David Jenn, for his patience and guidance throughout this period. I appreciate the time he spent sharing his knowledge with me, enabling me to understand the concepts and leading me in the right direction to achieve the results required.

I would like to thank Professor Terry Smith for readily agreeing to be my second reader. His comments and suggestions definitely added clarity to the thesis.

Special thanks to Dr. James Calusdian for building the rotator to support the collection of data for this thesis, which established the foundation for me to better understand the issues.

My deep appreciation goes to Mr. Robert Broadston for his constant assistance throughout this journey in providing his laboratory experience and tools for the thesis. Final measurements of the model in various configurations and angles would not have been possible if he had not built the supporting frame for the radar system.

Thanks also go to my beloved wife, Ms. Jolene Ge, for her love and unwavering support for my studies here at NPS. Thank you for taking good care of my two kids, Joel and Charmaine, back in Singapore so that I could fully focus on my studies here. This journey would not be possible without you.

Lastly, I thank the Lord Jesus Christ for His blessings in the completion of this master's degree.

THIS PAGE INTENTIONALLY LEFT BLANK

I. INTRODUCTION

A. OVERVIEW

It is known that greenhouse gases such as water vapor, nitrous oxide, methane, and carbon dioxide are major contributors to global warming. Ever since the industrial revolution that began in the 1760s, human activities have been releasing increasing amounts of carbon dioxide into the atmosphere every year. A large percentage of these emissions comes from the burning of fossil fuels to generate electricity or energy for our everyday needs [1]. In order to reduce harmful carbon emissions from the combustion of hydrocarbons, various cleaner alternatives for generating electricity are being explored and implemented. Harnessing wind energy using wind turbines (WT) is one of them.

The concept of harnessing wind energy in the United States is not something new, as it has been around since the establishment of U.S. Wind Engine Company in the 1850s, and, more recently, with the first large wind farm installed in California in 1980 [2]. The growth of wind farms over the last 15 years has been exponential with the cumulative wind power capacity increasing nearly 30 times or more in MW since 1999, as illustrated in Figure 1 [3].

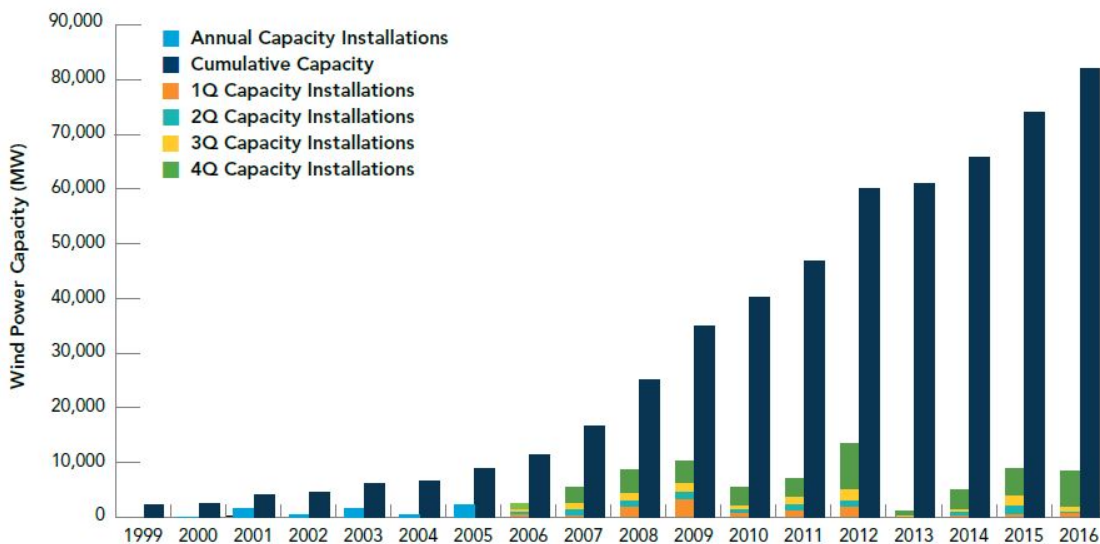


Figure 1. Wind Power Installation Capacity from 1999 to 2016. Source: [3].

B. RADAR INTERFERENCE FROM WIND FARMS

There are also challenges that come with the benefits of WTs. As the size and number of wind turbines increase, their operation can affect the military readiness of the surveillance radar installations near wind farms and the proper functioning of other commercial systems such as Air Traffic Control (ATC) Radar and Weather Radar, especially when the wind farms are within the radar line-of-sight (RLOS) [4]. One such example of radar interference is shown in Figure 2. The Doppler returns from a wind farm of 36 wind turbines negatively affect the Doppler weather radar's ability to provide accurate precipitation forecasts and advanced severe weather warnings, which has safety implications [5].

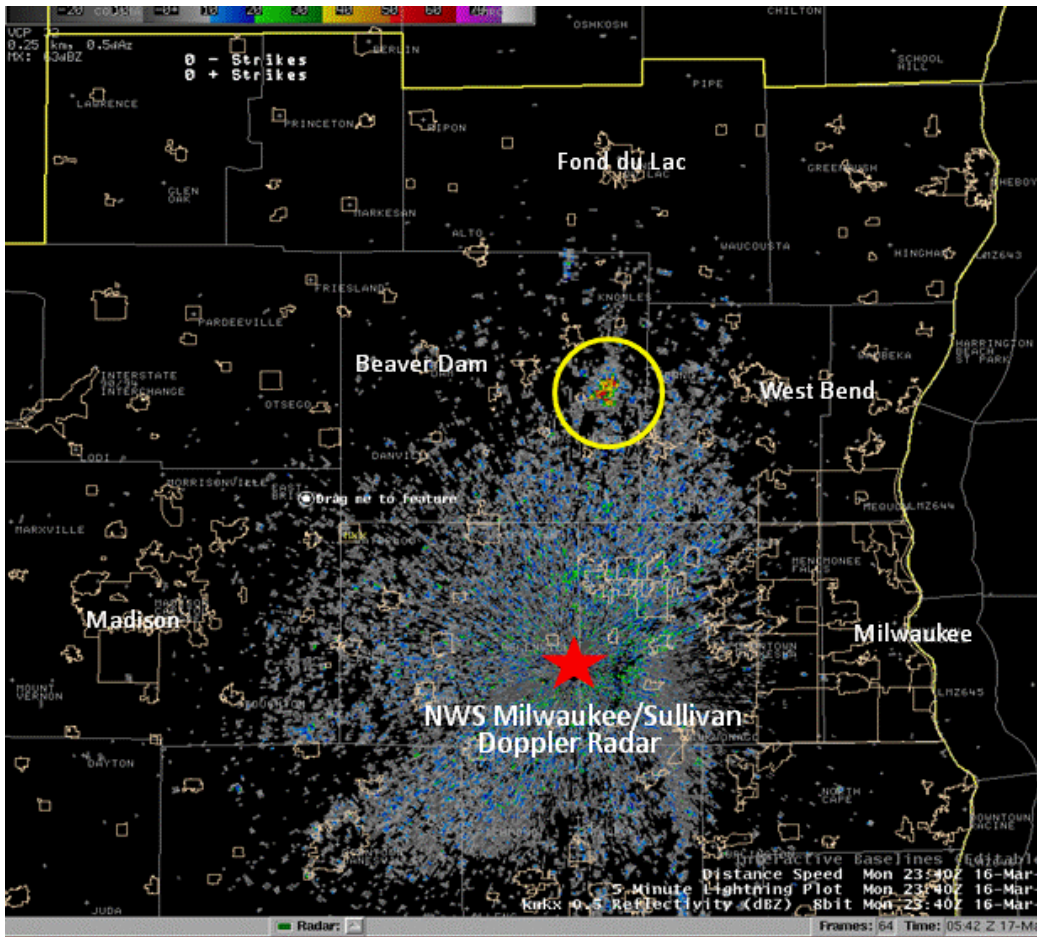


Figure 2. Doppler Returns from Wind Farms (yellow circle) on the Weather Radar Display. Source: [5].

C. MITIGATION APPROACHES

In order to mitigate the Doppler interference from the WTs, working groups have been formed to conduct studies to formulate strategies to overcome unintended interference. In general, there are three mitigation approaches, which are described in the following paragraphs.

1. Siting Options

A terrain survey can be conducted to determine a location's suitability for wind farms. With the height and radar-cross section (RCS) of wind turbines known, calculations can be conducted to determine whether the Doppler returns from the wind farms are small enough to avoid having an impact on the radar systems within the wind farms' vicinity [6]. An elevated terrain between the wind farms and radar sites can also serve as an effective obstacle to attenuate any Doppler returns. As such, advance planning for the location of wind farms can reduce or eliminate any impact to the radar operations.

2. Radar Options

For situations where wind farms affect current radar operations, it is possible to make certain adjustments or modifications to the radar systems. Antenna tilting can reduce the returns from the wind farms, for example, but if the RCS of the wind turbine is very large, a large tilt is needed, and this adversely affects the detection performance of low altitude air targets [6]. Modifications can also be made to the processing and tracking algorithms for the system to distinguish between the static returns from the wind farm clutter and valid returns from moving targets of interest.

A secondary radar system known as "fill-in" or "gap filler" radar can be installed in the vicinity to provide additional coverage after a terrain survey has been carried out. These two systems can be linked up to complement the primary radar through data fusion (see Figure 3) and filtering processing to allow the display of targets detected over the wind farm [6].

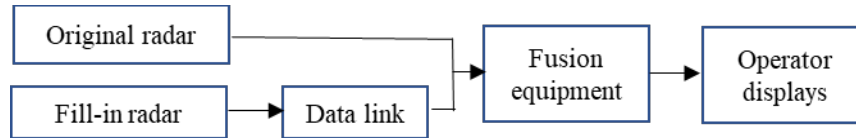


Figure 3. Data Fusion Architecture. Source: [6].

3. Wind Turbine Options

Lastly, it is possible to modify the wind turbine in terms of the structural design and materials used in order to reduce its RCS. The shape of turbine towers and nacelles can be designed such that any radio waves are reflected away from the radar. Furthermore, coating the surface of the turbine blades with radar absorbent material (RAM) can reduce the strength of the reflected signal back to the radar [6].

D. INTERFERENCE REDUCTION TECHNIQUES

As discussed earlier, there are various options available to mitigate the interference from the wind turbine; more details on modifications to the physical structure of the wind turbine to reduce the interference are now discussed. The RCS of the wind turbine has been investigated in [7]. It was found that in the static condition (fixed rotor position), the tower was the major contributor to interference at approximately 75% of the overall RCS, with the blades being the next major contributor at around 15%. Even though the blade contribution is small, its RCS is still much larger than that of targets-of-interest.

1. RCS Reduction for Tower and Blades

RAM can be applied to the tower easily and can potentially reduce the RCS up to 20 dB, but issues such as durability of the RAM material in an exposed environment and the additional cost and weight to the structure tend to negate the benefits. It was found that a conical structure tower replacement can reduce the RCS up to 43 dB. Since the blades are already optimally designed to capture the wind, however, it is not practical to change their shape. Alternatively, research shows that by applying a modified Salisbury screen-based absorber, it is possible to achieve an RCS reduction of around 15 dB for the blades [7].

2. Addition of Shroud and Wire Grid Screen

Studies have been conducted in [8] for different models of shrouds on their effectiveness to increase the wind capturing efficiency. With proper design on the profile of the shroud, a smaller inlet opening gradually flared to a bigger outlet, as shown in Figure 4, can increase the wind flow through the shroud by 28%. In contrast, the use of a common window screen (1.0-mm openings) at the inlet disrupts the pressure, preventing the wind turbine from operating efficiently. Use of mesh with a coarser weave (larger openings) was not investigated in [8].

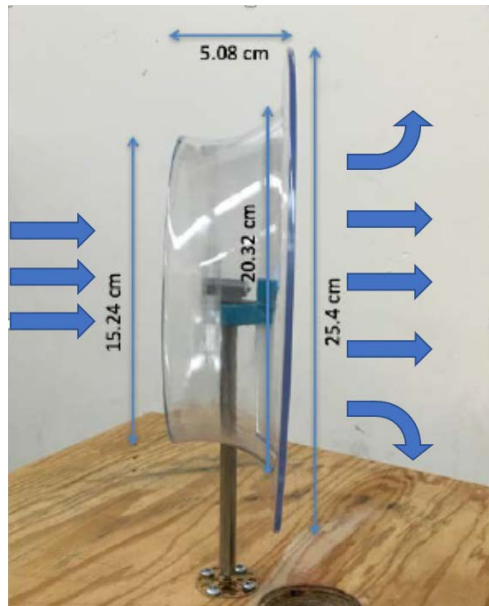


Figure 4. Shroud Model Used to Investigate Wind Capturing Efficiency.
Source: [8].

Wire grids have been frequently used to represent solid conducting surfaces; and when the spacing between the wires is small relative to the wavelength of the incident wave, the reflection coefficient is approximately one [9]. This means that by placing a screen of appropriate mesh size in front of a wind turbine, we can cause the electromagnetic waves transmitted by a radar to be reflected by the screen before they reach the blades, thereby reducing the Doppler return. Too coarse a mesh with respect to the radar wavelength renders the screen ineffective, and too fine a mesh might affect the

performance of the wind turbine in capturing the wind for power generation as found in [8].

An important frequency band for radar applications is the X-band (8–12 GHz). At this frequency, a metallic screen with openings of 0.5 inches by 0.5 inches or smaller should yield a reduction of Doppler return as the wavelength is 3.06 cm (1.2 inches) for a 9.8-GHz radar system.

E. RELATED WORKS

Radar signature measurement for a new model of wind turbine lens has been carried out in [10] in a setup that requires an area with a dimension of a football field. RCS and Doppler analysis have been carried out to determine the variations in RCS and Doppler shift with and without a metallic mesh around the shroud. The result shows that it is possible to achieve a radar return reduction of approximately 10 to 15 dB by fitting the metallic mesh around the shroud. On a smaller scale, the Doppler due to the wind turbine scattering was investigated in [11] by comparing the simulation result using Numerical Electromagnetics Code (NEC) to measurements conducted in the laboratory on a scaled-down wind turbine model. From the result, the Doppler features of a scale-model turbine are comparable to those reported for a large wind turbine. It was also observed from the Doppler signature that the shape and spacing of the blade flashes are related to the shape of the turbine blade.

F. THESIS OBJECTIVES

The objective of this thesis research is to validate the effectiveness of a shroud with metallic screens (one with 0.5 inches by 0.5 inches mesh and another with 1.0-mm by 1.0-mm mesh) in the reduction of Doppler interference for a scaled-down wind turbine model. The wind turbine is first simulated using a rotating arm with a metallic ball attached at one end (rotator) to generate the Doppler return. Doppler shift measurements are then carried out using a software-defined radar (SDR) through the transmission of a continuous wave (CW) signal. Post processing of the collected data (in the form of in-phase (I) and quadrature (Q) data) was carried out using MATLAB to generate the micro-Doppler signature [12]. Subsequently, we added a shroud and screen to determine their

effectiveness in Doppler suppression. Finally, we performed similar measurements on a wind turbine model in Port Hueneme, CA, for comparison.

G. THESIS OUTLINE

The organization of the thesis is as follows. In Chapter II, the background and concepts related to the understanding of the topic, such as CW radar operation and its performance characteristics, are introduced. Doppler clutter and its effect from WTs is discussed to illustrate the motivation of this thesis. Doppler processing of I and Q signals are also presented in Chapter II. Simulation results using the software Computer Simulation Technology (CST) Microwave Studio (MWS) to estimate the insertion loss expected using the metallic screen and wire mesh and measurement results of the two types of models are presented in Chapter III. Finally, we present a summary of findings and conclusions obtained from the analysis, simulations, and measured results in Chapter IV, along with recommendations for future work.

THIS PAGE INTENTIONALLY LEFT BLANK

II. CW RADAR OPERATION AND WT RCS

A. CW RADAR OPERATION

For a target in motion, the electromagnetic energy reflected back to the CW radar receiver has a change in frequency compared to the transmitted frequency. This change in frequency, known as Doppler frequency [12], can be calculated as

$$f_D = \frac{2v_r f_o}{c}, \quad (1)$$

where v_r is the relative radial component of the velocity of the target, f_o is the transmitted frequency, and c is the speed of light. A closing target approaching the radar has positive velocity, resulting in a positive Doppler frequency. A negative Doppler frequency occurs for a receding target.

For the simple CW radar system shown in Figure 5, transmitted and received signals share a common channel. The received signal is mixed with the transmitted signal at the detector, and the Doppler frequency is extracted after the Doppler filter.

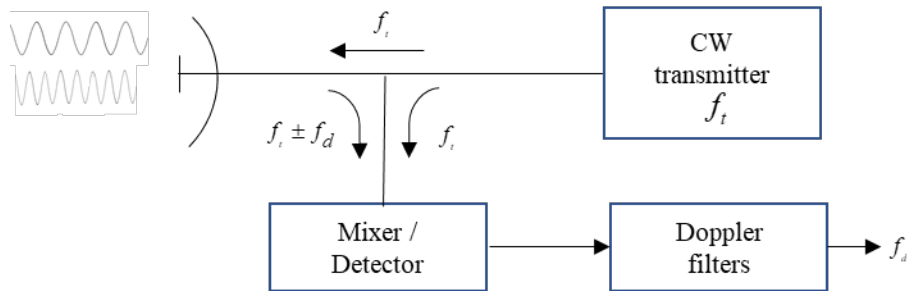


Figure 5. Simple CW Radar Block Diagram. Source: [13].

The received signal can be in the form of I and Q components, where the Doppler shifts can be extracted using a quadrature detector, as shown in Figure 6.

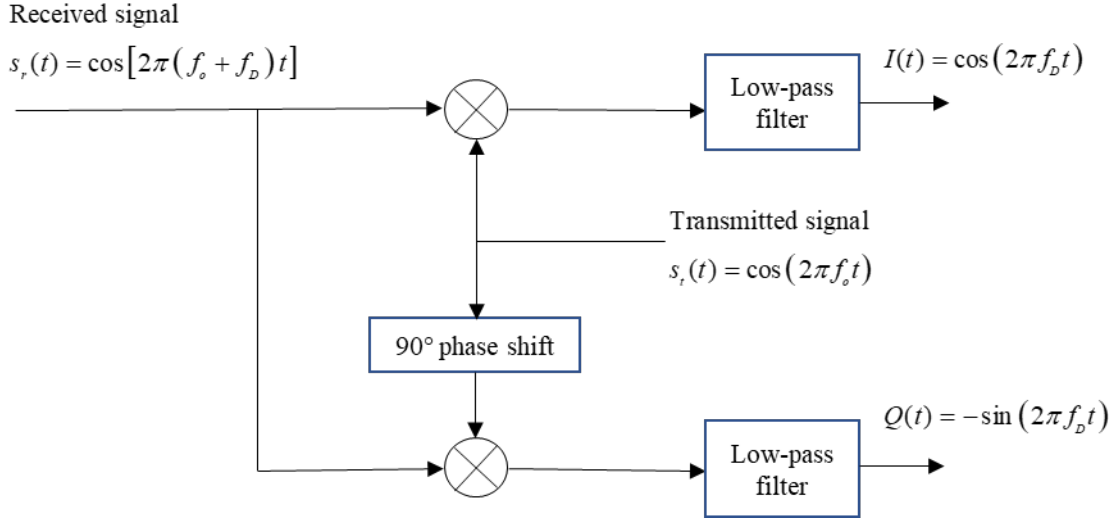


Figure 6. Doppler Shifts Extracted by a Quadrature Detector. Source: [12].

B. INTERFERENCE FROM WIND TURBINES

The characteristics and features of the wind turbine and how its operation can affect the operation of a radar system are discussed in more detail in this section. The main function of radar is to detect and track targets of interest based on the information extracted from the reflected signal. When undesirable clutter or noise is received together with the reflected signal, the processor's ability to obtain the required target-of-interest information is affected. The strength, or magnitude, of the reflected signal and the Doppler frequency shift from the moving target are two of the basic features the radar uses to detect and track the target.

1. Radar Cross Section of the Wind Turbine

A typical horizontal wind turbine mainly comprises the rotor, which catches the wind; the nacelle, which houses the turbine to convert kinetic energy to electrical energy; the tower structure supporting the rotor and nacelle; and the foundation for the tower. Due to the large size of the wind turbine relative to the radar's wavelength, it has a large RCS, which gives a strong electromagnetic signal return to a radar system.

The large RCS from the wind turbine results in a large amount of unwanted clutter. The clutter, when added onto the noise level, can potentially mask the returns of any

smaller targets-of-interest in the vicinity [13]. The large returns to the radar can also take multiple paths (reflections), thus appearing as “ghost” targets on the radar display [14]. These “ghosts” affect the radar’s ability to unambiguously detect and discriminate targets-of-interest. As pointed out previously, the static (non-time varying) components of the RCS are more easily handled by the processor than are the Doppler returns from the moving WT parts.

2. Doppler Frequency Shift from the Wind Turbine

The main moving parts of the wind turbine, which are the rotating blades, generate strong Doppler frequency shift, causing issues for the radars to discriminate between the wind turbine and moving targets. Depending on their length, size, and shape, rotating blades can produce a tip velocity of 50 to 150 m/s depending on the prevailing wind speed [12]. Accuracy of wind estimates from the Doppler weather radar can also be affected as the Doppler frequency shift can be processed as wind speed.

C. SYSTEM DESCRIPTION AND SIGNAL PROCESSING

The system description of the radar system used to collect the data and the process of extracting the Doppler information for further analysis are discussed in this section.

1. Software-Defined Radar

In this thesis, data is collected using the SDR-KIT 980AD module from Ancortek, Inc. SDR-KIT 980AD is an X-Band, software-defined radar with most of the processing occurring on a field-programmable gate array (FPGA), while the computer connected to it handles the controls and display of measured results. As highlighted in [15], the main advantage of using an SDR is its flexibility to operate multiple modes using the same hardware with only changes to the processing algorithm implemented in the FPGA. This leads to faster development and reduced cost. The SDR system block diagram is shown in Figure 7.

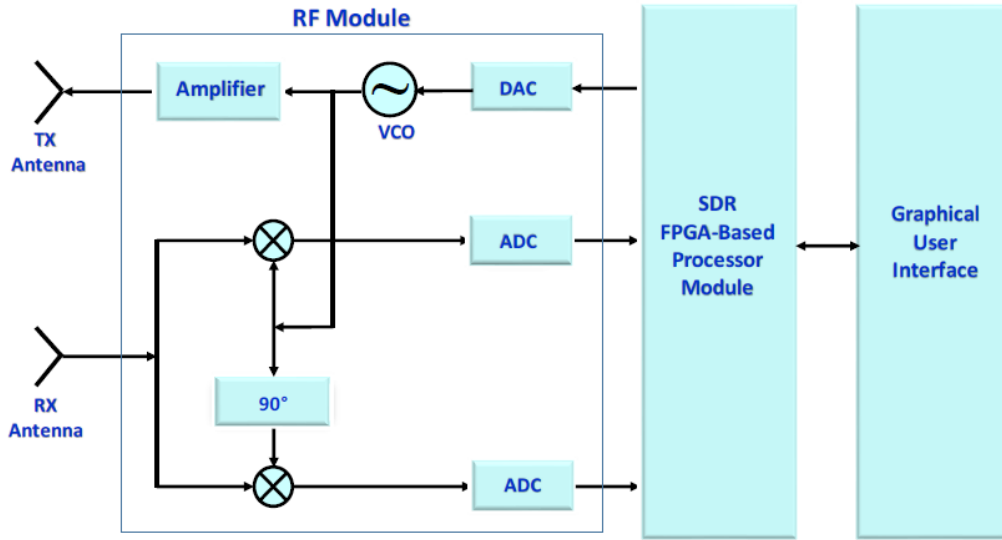


Figure 7. SDR System Block Diagram. Source: [16].

As demonstrated in [17], an SDR-KIT 980AD can accurately collect data for the processing of micro-Doppler signatures. The system uses a graphical user interface (GUI) to control the transmission parameters as well as the display settings of the SDR on the computer, which is connected to the SDR via a universal serial bus (USB) cable. The SDR FPGA-based processor module generates digital samples of control voltage that are converted to an analog control voltage by a digital-to-analog converter (DAC). The DAC drives the voltage-controlled oscillator (VCO), which generates the desired type of waveform for transmission. The output signal of the VCO is amplified before it is transmitted. At the same time, the output signal is also fed to the receiver channel to be mixed with the received signal to obtain the I and Q data. The I and Q data are then digitized through an analog-to-digital converter (ADC) and displayed in the GUI or stored in the computer for post-processing. The output of the mixer in the receive chain is digitized and streamed to the host computer for further processing. Some of the key system parameters for the SDR-KIT 980AD are shown in Table 1. Instead of the patch antennas that came with the system, our research used two horn antennas with higher gain [18].

Table 1. SDR-KIT 980AD Parameters. Source: [16].

Parameter	Unit	Value
Waveforms	-	FMCW / CW / FSK
Center Frequency	GHz	9.8
Power	dBm	18
Bandwidth	MHz	100, 150, 300, 400
Sweep Time	ms	1, 2, 4, 10
Number of Samples per Sweep	-	128, 256, 512, 1024
Horn Antenna Gain [18]	dB	20

2. Extracting Doppler Frequency Shift

As described in Figure 6, the Doppler frequency generated by a target of interest can be extracted by mixing the transmitted and received signals to get the baseband I and Q data. The transmitted signal is of the form [12]

$$s_t(t) = \cos(2\pi f_0 t). \quad (2)$$

The received signal will have amplitude a with a phase shift due to the motion of the moving target.

$$s_r(t) = a \cos(2\pi(f_0 + f_D)t) \quad (3)$$

The received signal is mixed with the transmitted signal and undergoes low-pass filtering to get the I signal and the Q signals. The I signal before filtering is

$$I' = \frac{a}{2} \cos(4\pi f_0 t + 2\pi f_D t) + \frac{a}{2} \cos(2\pi f_D t). \quad (4)$$

The I signal after low-pass filtering is

$$I = \frac{a}{2} \cos(2\pi f_D t). \quad (5)$$

The Q signal before filtering is

$$Q' = \frac{a}{2} \sin(4\pi f_0 t + 2\pi f_D t) - \frac{a}{2} \sin(2\pi f_D t). \quad (6)$$

The Q signal after filtering is

$$Q = -\frac{a}{2} \sin(2\pi f_D t). \quad (7)$$

Equations (5) and (7) combined give the complex Doppler signal

$$s_D(t) = I(t) + jQ(t) = \frac{a}{2} e^{-j(2\pi f_D t)}. \quad (8)$$

3. Time-Frequency Analysis of Doppler Signature

The Fourier Transform (FT) is a very useful and powerful tool to process signals and understand their frequency characteristics. The definition of the FT of a signal $x(t)$ is given as [19]

$$X(f) = \text{FT}\{x(t)\} = \int_{-\infty}^{+\infty} x(t) e^{-j2\pi ft} dt, \quad (9)$$

where FT of the signal is carried out as a whole.

As the reflected signal from the rotator or wind turbine is a signal that varies over time, taking the FT of the whole sampling duration does not allow us to observe the characteristics at different time intervals. In this case, the short-time Fourier Transform (STFT) [19] is used to process the received signal and display it as a spectrogram. The STFT performs the Fourier Transform on segmented portions of the signal using a time-limited window function and is defined as [19]

$$X(\tau, f) = \text{STFT}\{x(t)\} = \text{FT}\{x(t)w(t-\tau)\}, \quad (10)$$

where $w(t-\tau)$ is the window signal centered around the time variable τ depicted in Figure 8.

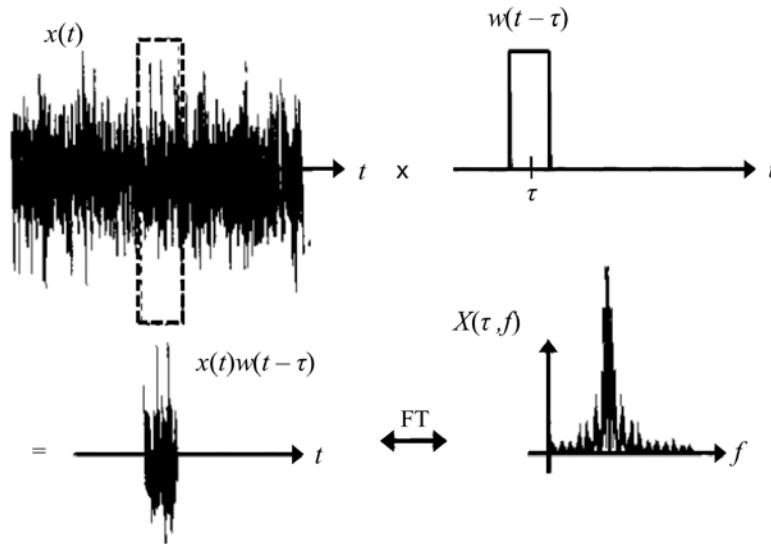


Figure 8. Short-Time Fourier Transform. Source: [19].

Taking Equation (10) into consideration, we expand the FT to get

$$X(\tau, f) = \int_{-\infty}^{+\infty} x(t)w(t-\tau)e^{-j2\pi ft} dt. \quad (11)$$

In using STFT, signal processing leads to time/frequency uncertainty due to the windowing. The frequency resolution is inversely proportional to the width of the window (observation time), as shown in Figure 9, using the example of a rectangular window.

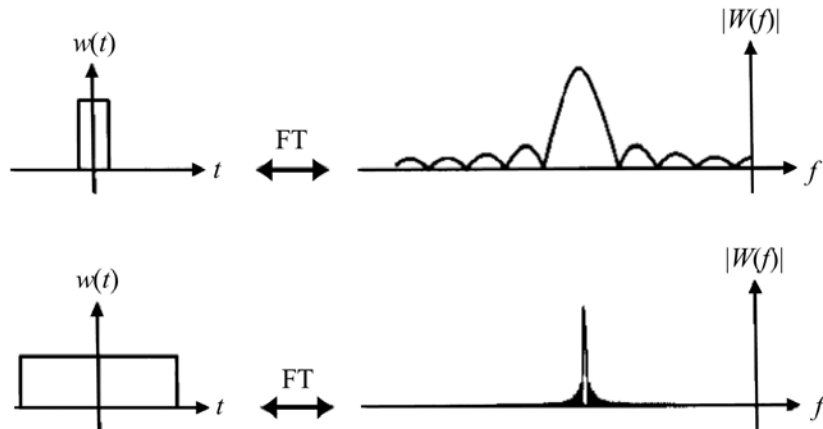


Figure 9. Time/Frequency Uncertainty of a Rectangular Window. Source: [19].

Gaussian windowing is typically used as it has been shown to give the best performance for time/frequency uncertainty, as shown in Figure 10 with a Gaussian window of the form [19]

$$w(t) = \frac{1}{\sqrt{\pi}} e^{-t^2}. \quad (12)$$

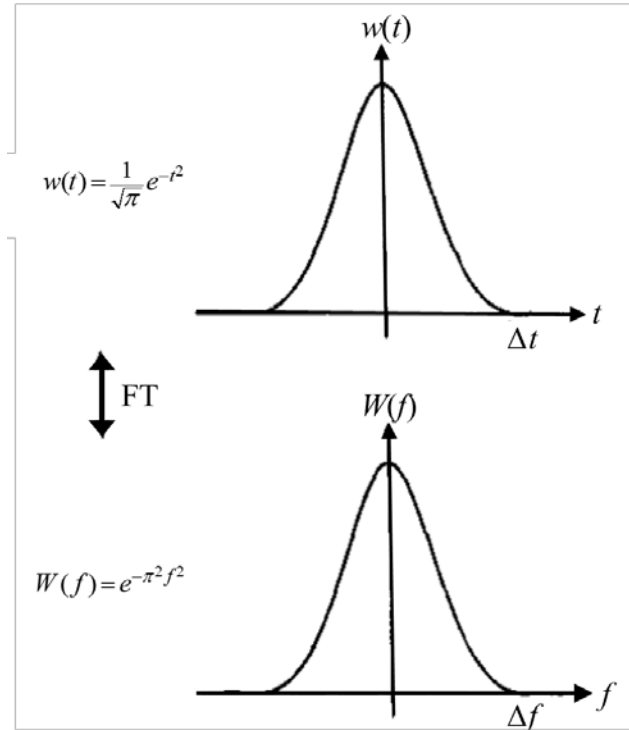


Figure 10. Best Time/Frequency Resolution with Gaussian Window.
Source: [19].

The received signal is sampled at a specific rate and is stored as complex I-Q data for post-processing. Before processing, the direct current (DC) bias of the received data is removed and separated into I and Q data before I-Q imbalance correction is carried out [20]. As the number of samples of the received signal collected are much greater than necessary, de-sampling by a factor of 2^N is performed to reduce the number of samples.

In this chapter, the operations of a CW radar system and the effects of the RCS and Doppler frequency shift from wind turbines on radar systems were discussed. Benefits of SDR and the use of the STFT to process the data to analyze the Doppler signature were presented.

In the next chapter, simulation and measurement results are compared to determine the effects of a shroud and screen in reducing Doppler interferences from a wind turbine.

THIS PAGE INTENTIONALLY LEFT BLANK

III. SIMULATION AND MEASUREMENT RESULTS

In this chapter, we present the results of simulations on screens to estimate the reduction in Doppler returns. Measurements are conducted on a rotator and a scaled WT, both with shroud, to verify the simulation data. The preparation work and setup for measurement are also presented in this chapter.

A. SIMULATION AND MEASUREMENT FOR THE SCREEN

CST Microwave Studio (MWS) simulations were carried out to estimate the insertion loss of a plane wave going through screens, and the results are compared against the actual measurements. The simulation is carried out using the Frequency Solver employing the Floquet Technique [9] (see Figure 11) as the screen or mesh can be considered as an infinite planar periodic structure. Computation of the fields and current only needs to be applied to one unit cell. The unit cell result is applied to obtain the total fields and currents for an infinite periodic structure.

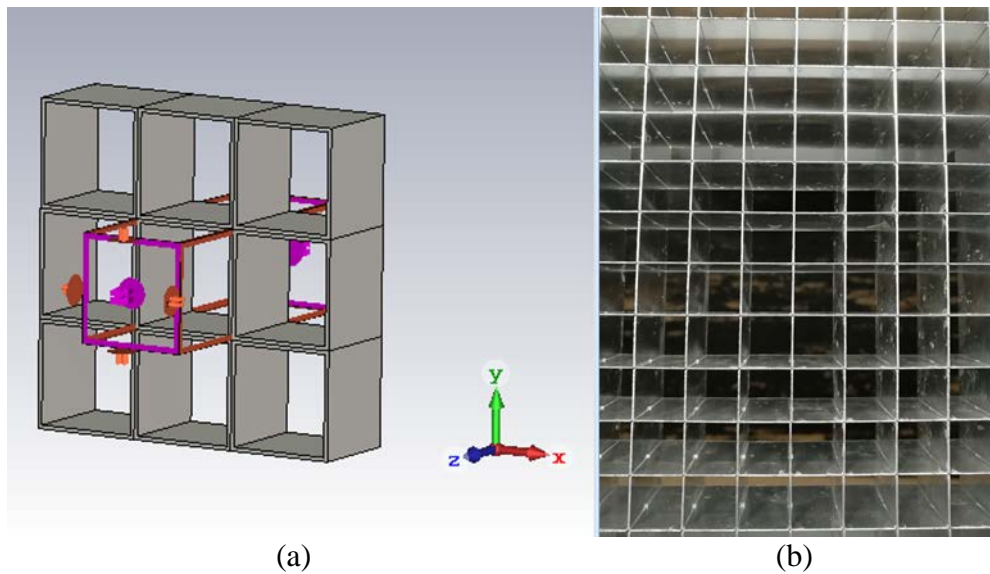


Figure 11. Estimating Insertion Loss of Plane Wave Passing through Screens:
(a) Simulation of Screen Using Floquet Technique (unit cell highlighted). (b) Photograph of Actual Screen

1. Simulation Result for Screen with 0.5 Inch by 0.5 Inch Opening

A one-way insertion loss of approximately 14 dB (see Figure 12) is expected for a 9.8 GHz signal normally incident on the screen shown in Figure 11b. For a monostatic radar, the return from blades behind the screen sees a two-way reduction (≈ 28 dB).

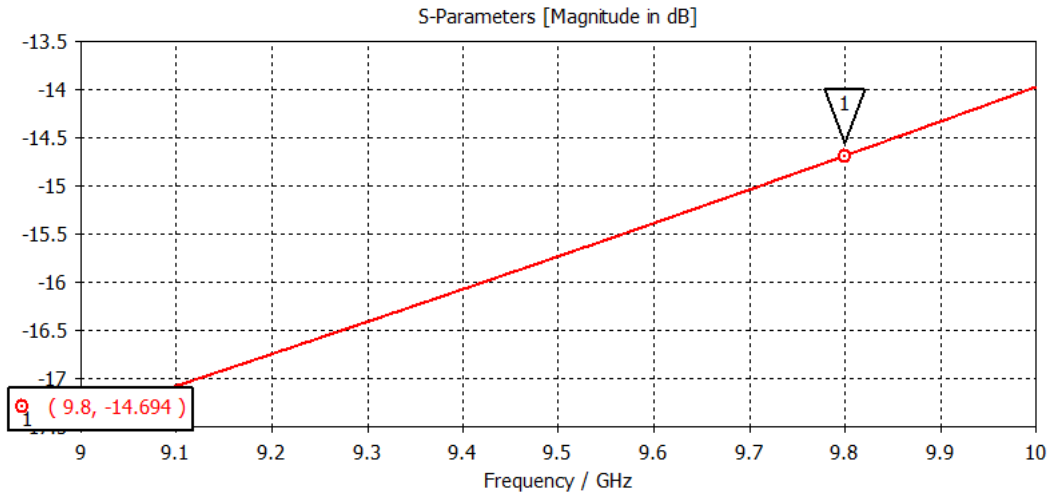


Figure 12. S11 Parameters for Screen with Opening of 0.5 Inches by 0.5 Inches

2. Simulation Result for Wire Mesh

A one-way insertion loss of approximately 29 dB (see Figure 13) is expected for a 9.8 GHz signal incident on the wire mesh as shown in Figure 14. The result seems to suggest a two-way loss of 58 dB, which might not be achievable as the simulation assumes the mesh is made up of perfectly conducting material with perfect connections at the wire junctions. The actual mesh does not have such features, and it can be expected that the actual loss will be less.

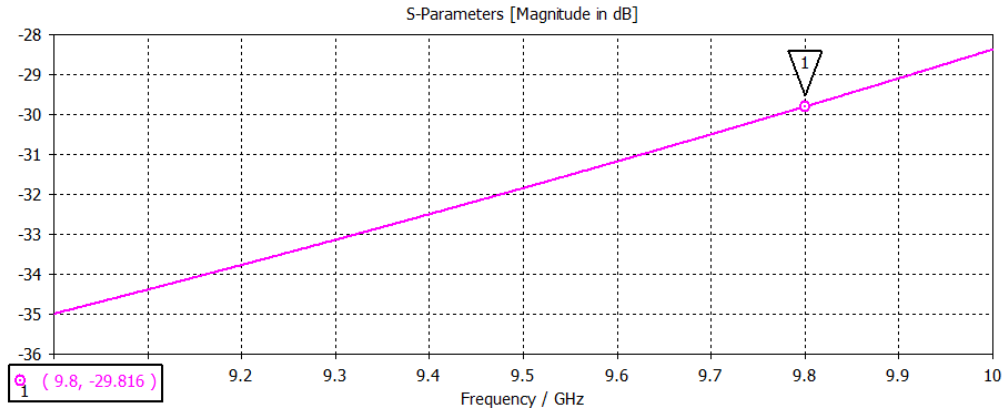


Figure 13. S11 Parameters for Mesh of 1.0 mm by 1.0 mm Opening

3. Insertion Loss Measurement for Wire Mesh

To verify the simulation data and obtain a better understanding of the effectiveness of the wire mesh (Figure 14), we performed an insertion loss measurement using the Labvolt antenna instrumentation. A CW signal at 9.8 GHz was fed to the transmit antenna, and the screen was placed between the transmitting and receiving antennas. Measurements were carried out as the receiving antenna makes a 360° rotation to capture the signal strength at various angles. The maximum signal strength occurred when the transmitting and receiving antennas were aligned with each other at 0° or 360°. A measurement made without the screen established the baseline signal level. Insertion loss can be obtained by taking the difference between the measurement with the wire mesh and the baseline measurement.

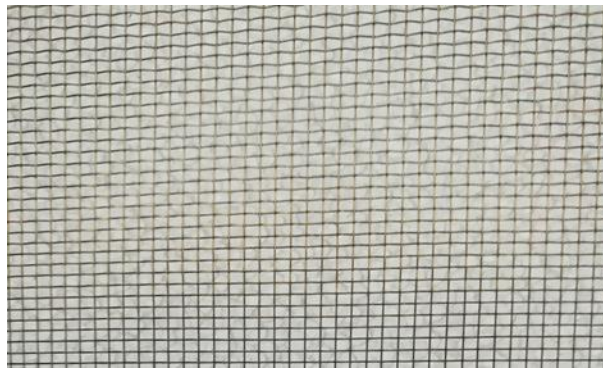


Figure 14. Wire Mesh of 1.0 mm by 1.0 mm Openings

An insertion loss of approximately 18 dB was obtained by comparing the differences between the measurement data shown in Figures 15 and 16. This is about 10 dB less than the MWS simulation. The measurement has errors (i.e., multiple reflections are present and leakage occurs around the sample). Additionally, the sample is not a perfect conductor with perfect contact at the junctions.

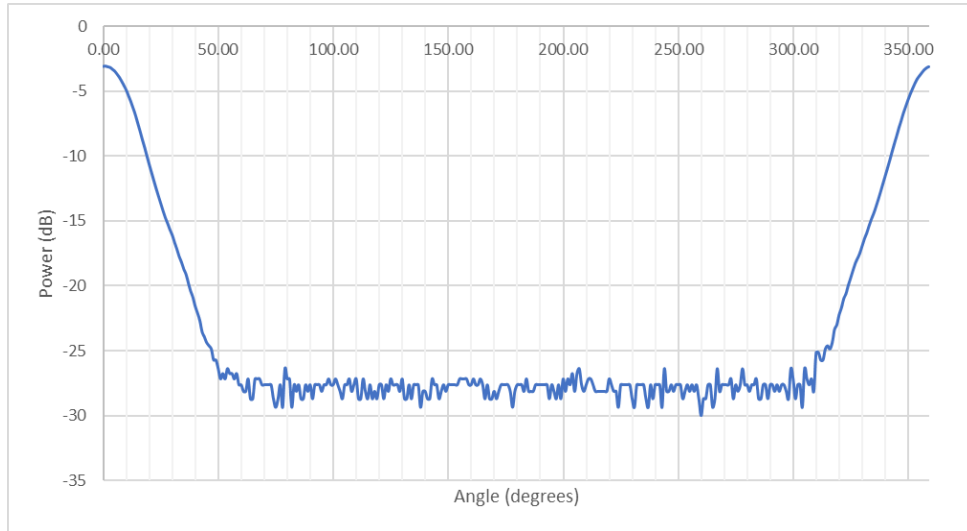


Figure 15. Baseline Measurement Using Labvolt Instrumentation

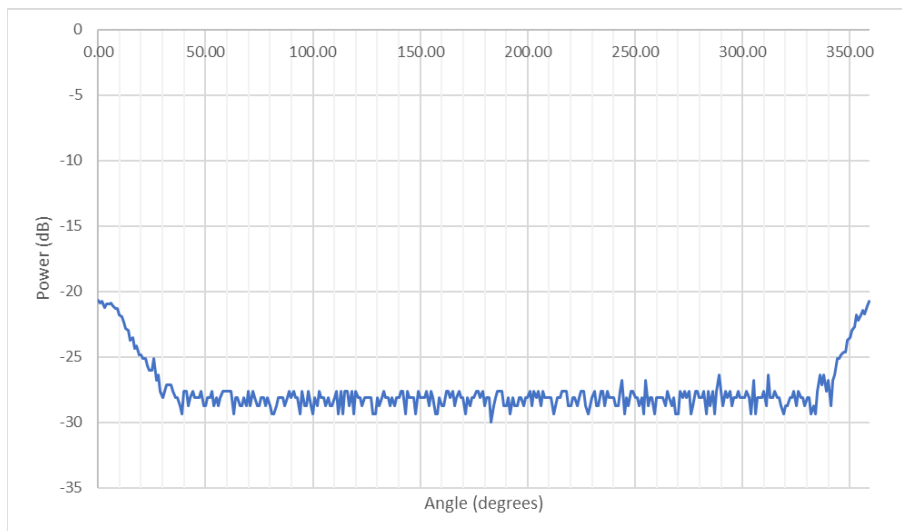


Figure 16. Measurement with Wire Mesh Using Labvolt Instrumentation

B. RADAR MEASUREMENT RESULTS

The preparation work before the actual data collection using the SDR and the methodology are discussed in this section.

1. Measurement Setup Using SDR

To determine the accuracy and capability of the SDR to measure the Doppler return frequency and the changes to amplitude of the signal returns, we devised the laboratory setup shown in Figure 17.

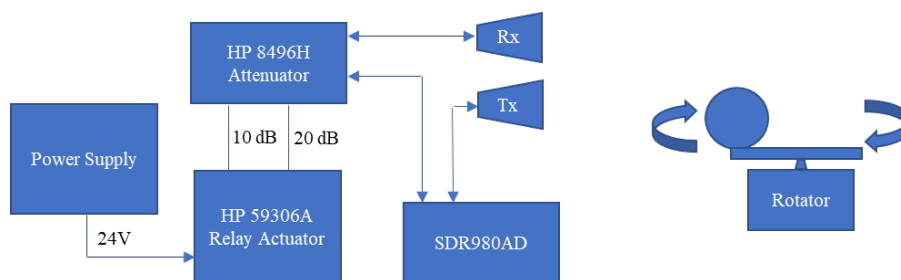


Figure 17. Equipment Setup to Determine Measurement Accuracy of SDR

The equipment includes the power supply to provide 24 Vdc to an HP 59306A relay actuator. The HP 59306A relay actuator selects the required relay to be energized for the attenuation required at the HP 8496H attenuator. The HP 8496H attenuator allows attenuation up to 110 dB for frequencies up to 18 GHz. In this setup, 10 dB and 20 dB attenuation cards in the HP 8496H are connected to the relay actuator for selection. The output of the receiving antenna is connected to the attenuator to apply the attenuation required before going back to the SDR980AD as data samples for post-processing.

During the measurement, the radar illuminates the rotator at a fixed distance of about 6.0 m and collects samples at 0 dB, 10 dB, 20 dB, and 30 dB attenuation levels for comparison. The rotation rate is about 50 rpm. The SDR is transmitting in CW mode with a sweep time of 1.0 ms and 128 samples collected per sweep. With a radius of about $r = 0.29$ m, the maximum radial velocity of the rotator in m/s is

$$v = 2\pi r \frac{\omega_{rpm}}{60}. \quad (13)$$

The maximum Doppler frequency can be calculated using Equation (1), which gives approximately 99.2 Hz. The results for different applied attenuation levels are shown in Figures 18 to 21.

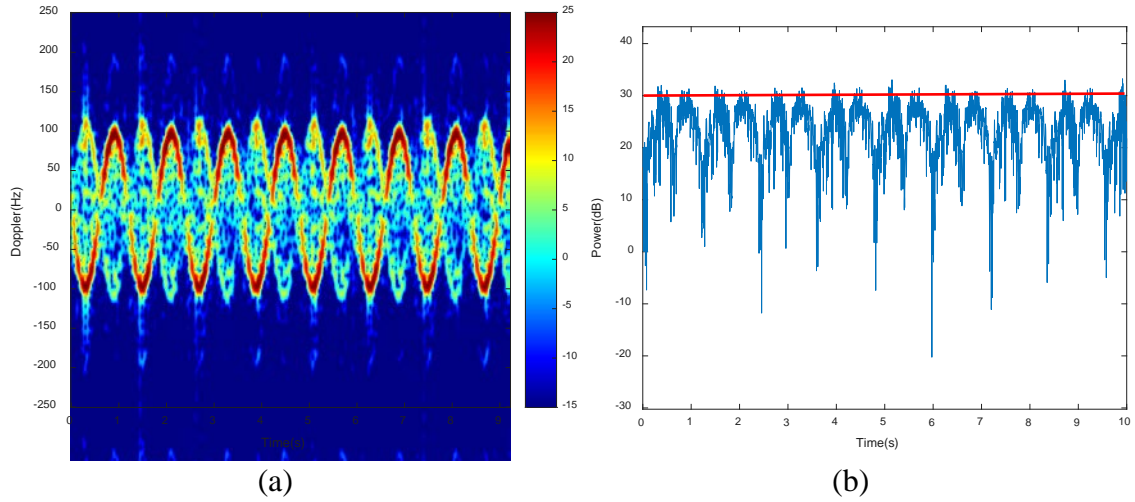


Figure 18. Received Signal in dB Versus Time with No Attenuation Applied: (a) Spectrogram and (b) Power

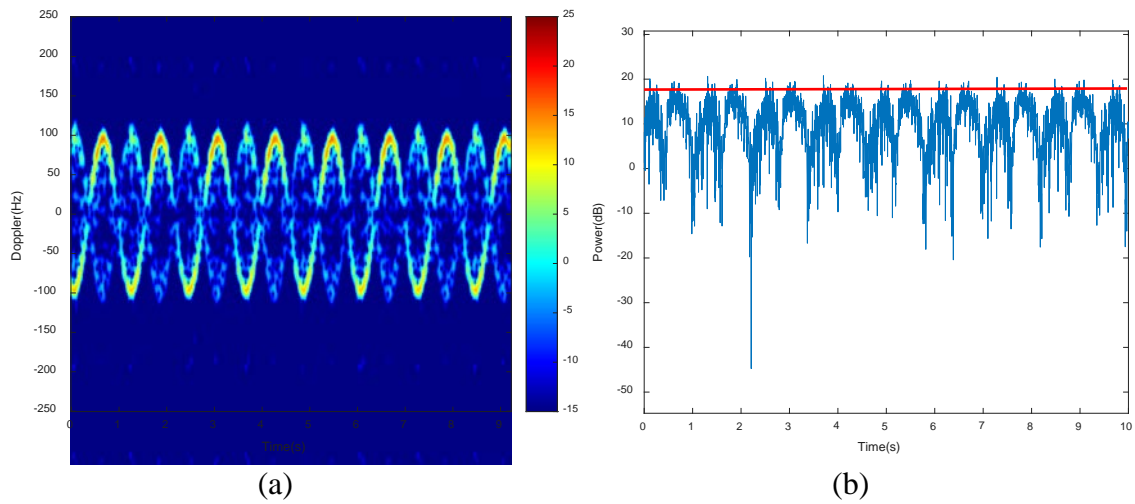


Figure 19. Received Signal in dB Versus Time with 10 dB Attenuation Applied: (a) Spectrogram and (b) Power

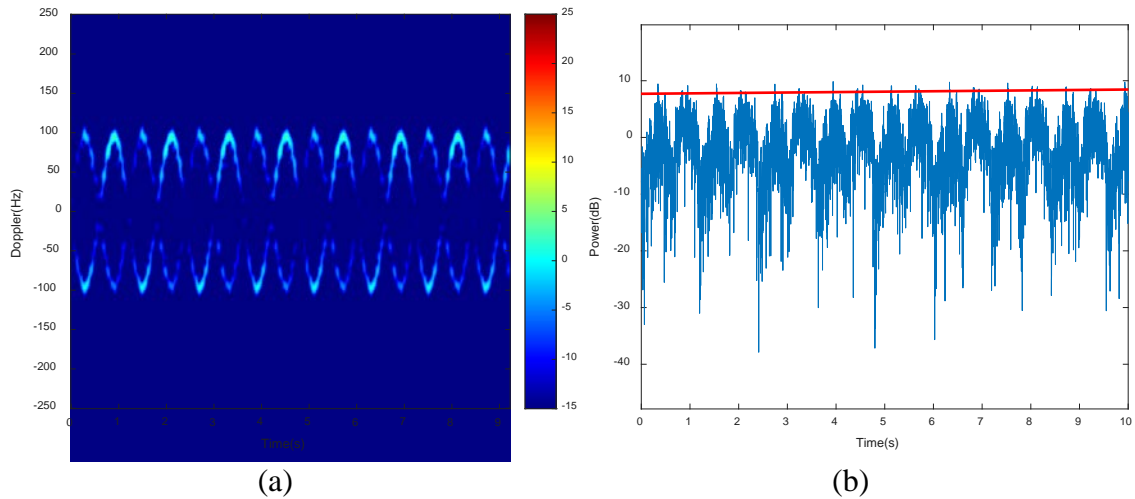


Figure 20. Received Signal in dB Versus Time with 20 dB Attenuation Applied: (a) Spectrogram and (b) Power

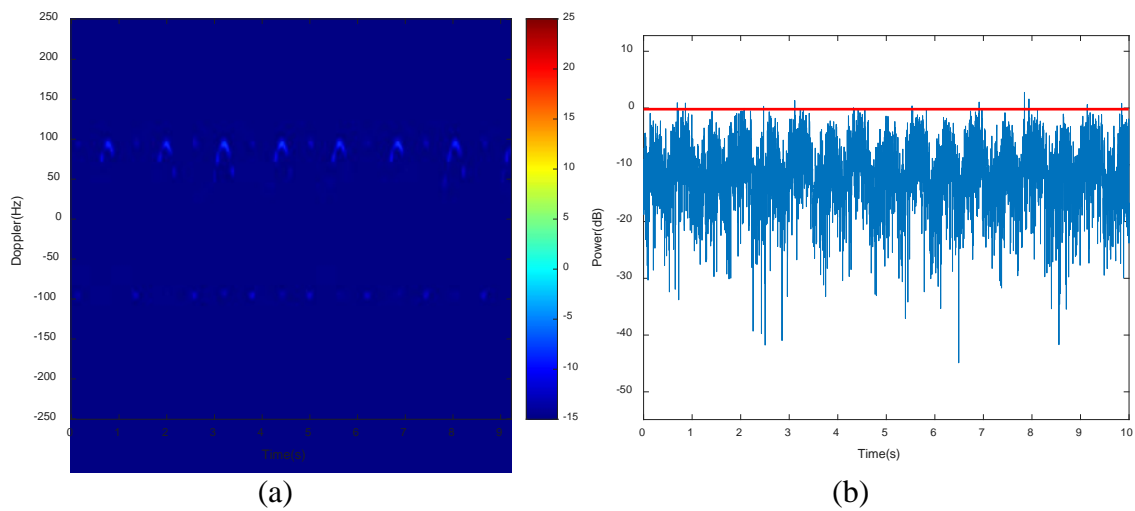


Figure 21. Received Signal in dB Versus Time with 30 dB Attenuation Applied: (a) Spectrogram and (b) Power

From the spectrogram in Figure 18, we observe the maximum Doppler frequency is approximately 100 Hz, which agrees reasonably well with the calculated value of 99.2 Hz. It can also be seen from the spectrograms in Figures 18 to 21 that the reduction in the strength of the Doppler signal power level is clearly a function of attenuation level. From the attenuator specifications [21], we observe the accuracy of the attenuation of 10 dB, 20 dB, and 30 dB is 0.5 dB, 0.7 dB, and 0.9 dB, respectively. The results from

Table 1 suggest that the attenuation accuracy does not meet the manufacturer's specifications. This can be due to several reasons such as the aging of components, additional loss due to cables and coupling, and other measurement errors; however, this exercise does show that any reduction of the returned signal due to the shroud and screen can be processed and presented in the form of a spectrogram and power plot.

Table 2. Result Summary for Different Attenuation Applied

Attenuation Applied	Maximum Power	Difference from 0 dB measurement
0 dB	30 dB	-
10 dB	19 dB	11 dB
20 dB	8 dB	22 dB
30 dB	0 dB	30 dB

2. Measurement Results for Metallic Ball on Rotating Arm

A structure was needed to mount the horn antennas and allow variable aspect angles to the rotator. The main design consideration is to ensure that the distance between the antenna and the rotator is sufficient to meet far-field conditions, which can be calculated using [22]

$$r > \frac{2D^2}{\lambda} \quad (14)$$

$$r > 5D \quad (15)$$

$$r > 1.6\lambda, \quad (16)$$

where r specifies the minimum distance required for far-field conditions and D is the maximum dimension of the antenna.

For transmission in the GHz region, Equation (14) is usually the limiting condition for the far-field condition. For a horn antenna with dimensions of 123.8 mm by 91.9 mm [18], a minimum distance of approximately 1.0 m is required between the antenna and rotator.

The structure allows for measurements to be made from angles of 0° to 60° offset from the rotator. At 0° , the antenna is at the center with the rotator directly below, as shown in Figure 22, and the 60° offset angle is shown in Figure 23. Measurements are carried out at increments of 10° to 60° for four different configurations, and samples for a period of 10.0 s are stored for post-processing. The results from the rotator itself form the point of comparison for the other configurations.

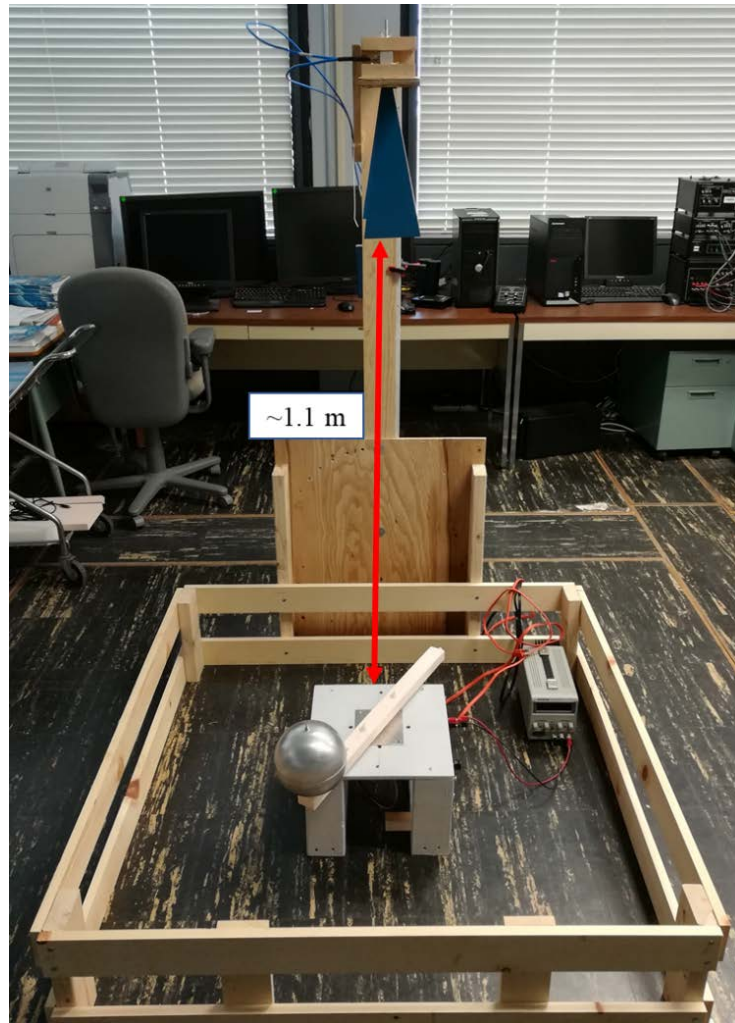


Figure 22. Measurement at 0° Offset Angle

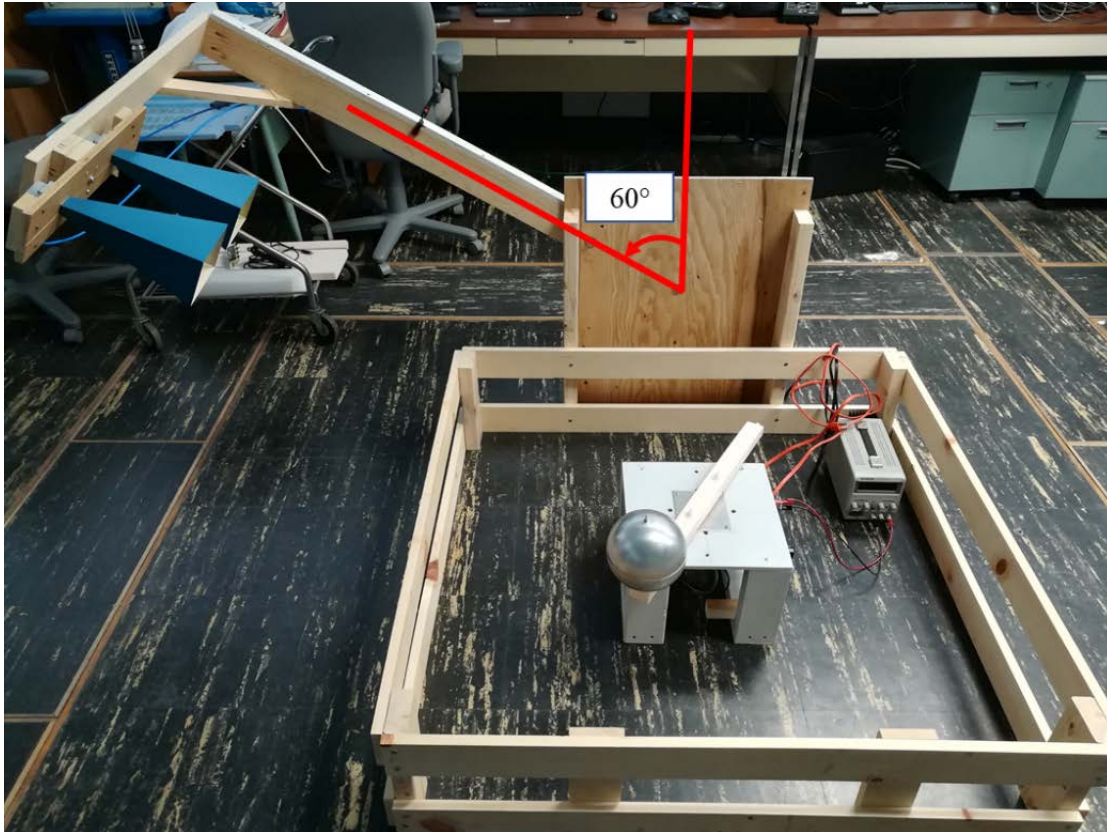


Figure 23. Measurement at 60° Offset Angle

From the spectrogram shown in Figure 24, we observe the Doppler frequency is the highest when the offset angle is the largest. This is related to the $\sin \theta$ factor where the maximum Doppler frequency of 158.8 Hz occurs when the offset is at 90° with the rotator rotating at 80 rpm. It is worthwhile to note that the rotator rpm is not always constant at 80 rpm but fluctuating between 76 rpm to 84 rpm, giving a maximum Doppler between 150.7 Hz to 166.5 Hz. A comparison between the theoretical and measured Doppler frequencies is provided in Table 3.

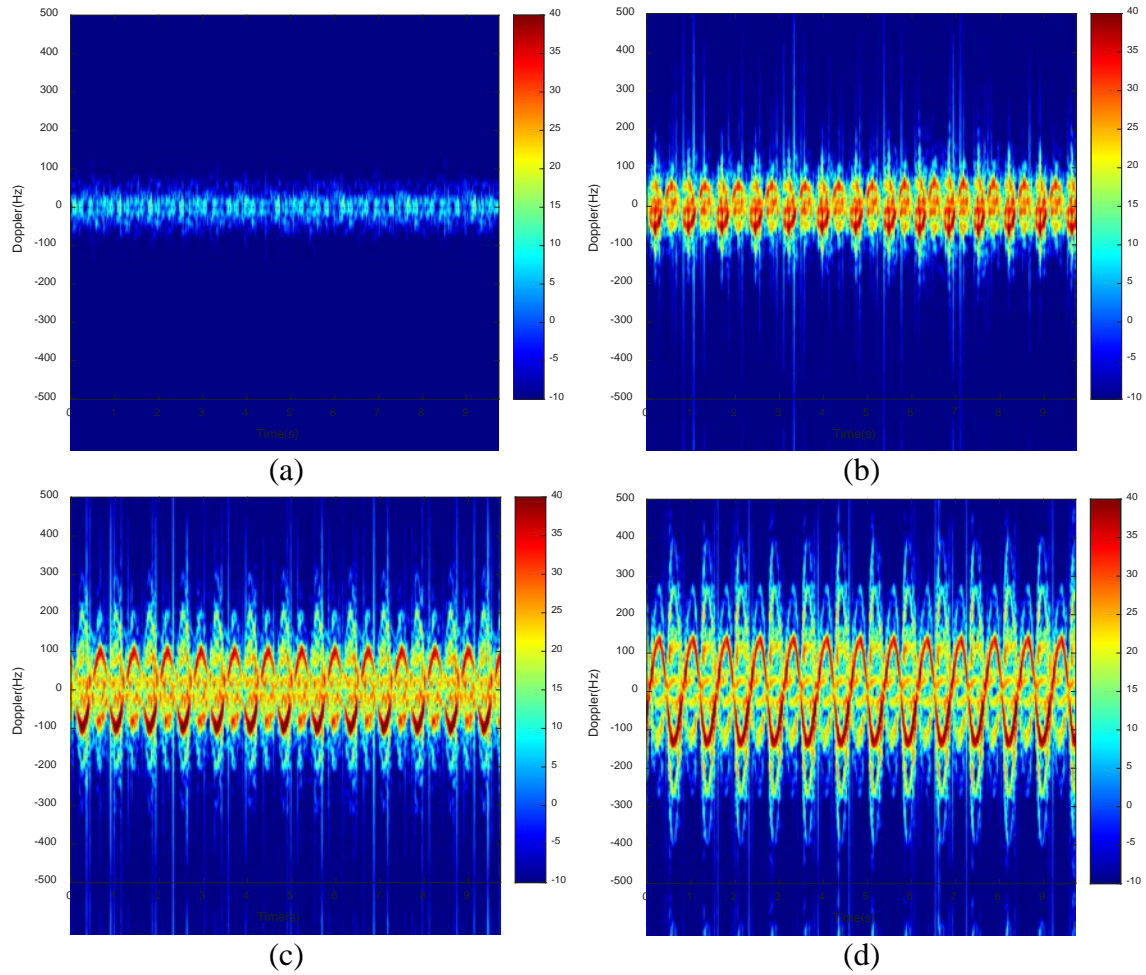


Figure 24. Doppler Spectrogram (dB) for Antenna at: (a) 0° , (b) 20° , (c) 40° , and (d) 60° Offset Angle from Rotator at 80 rpm

Table 3. Comparison between Theoretical and Measured Doppler Frequencies

Offset ($^\circ$)	Theoretical Doppler (Hz)			Measured Doppler (Hz)
	$f_{Dmax}= 150.7$ Hz	$f_{Dmax}= 158.8$ Hz	$f_{Dmax}= 166.5$ Hz	
0	0.0	0.0	0.0	13
10	26.2	27.6	28.9	23
20	51.5	54.3	56.9	58
30	75.4	79.4	83.3	80
40	96.9	102.1	107.0	107
50	115.4	121.6	127.5	126
60	130.5	137.5	144.2	139

The theoretical Doppler and the measured Doppler return frequencies agree reasonably well for most angles (especially with the upper theoretical limits) as seen from Figure 25, except in the region between 0° and 10°. There are some possible factors that contributed to the Doppler return frequencies observed: the antenna and the rotator are not perfectly aligned such that the rotator is centralized between the antennas; placement of the metallic ball is not exactly at equal distance from the other end on the rotator arm; vibrations from the rotator leading to micro-Doppler generated and received by the antenna; and lastly, as the environment is not padded with absorbing material and the rotator is seated near to the floor, reflections from the rotator’s movement may be contributing to the discrepancy in the Doppler return frequency comparison.

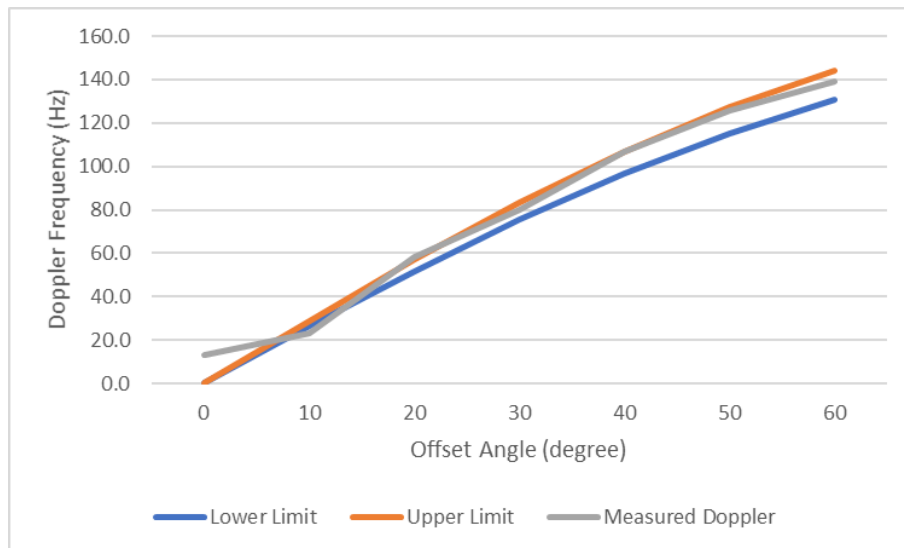


Figure 25. Comparison of the Values between Theoretical Doppler and Measured Doppler Frequencies for Rotator

The total power of the received signal in the receiver’s passband (10 MHz) at different antenna offsets was processed, and a comparison was made based on the peak value of the power envelope. Other than the case when the antenna is at 0° offset, which is about 20 dB, the power generally falls within 45 dB to 50 dB, as shown in Figure 26. The results depicted in Figures 24 and 26 serve as the baseline for comparison with those for the shroud and screen.

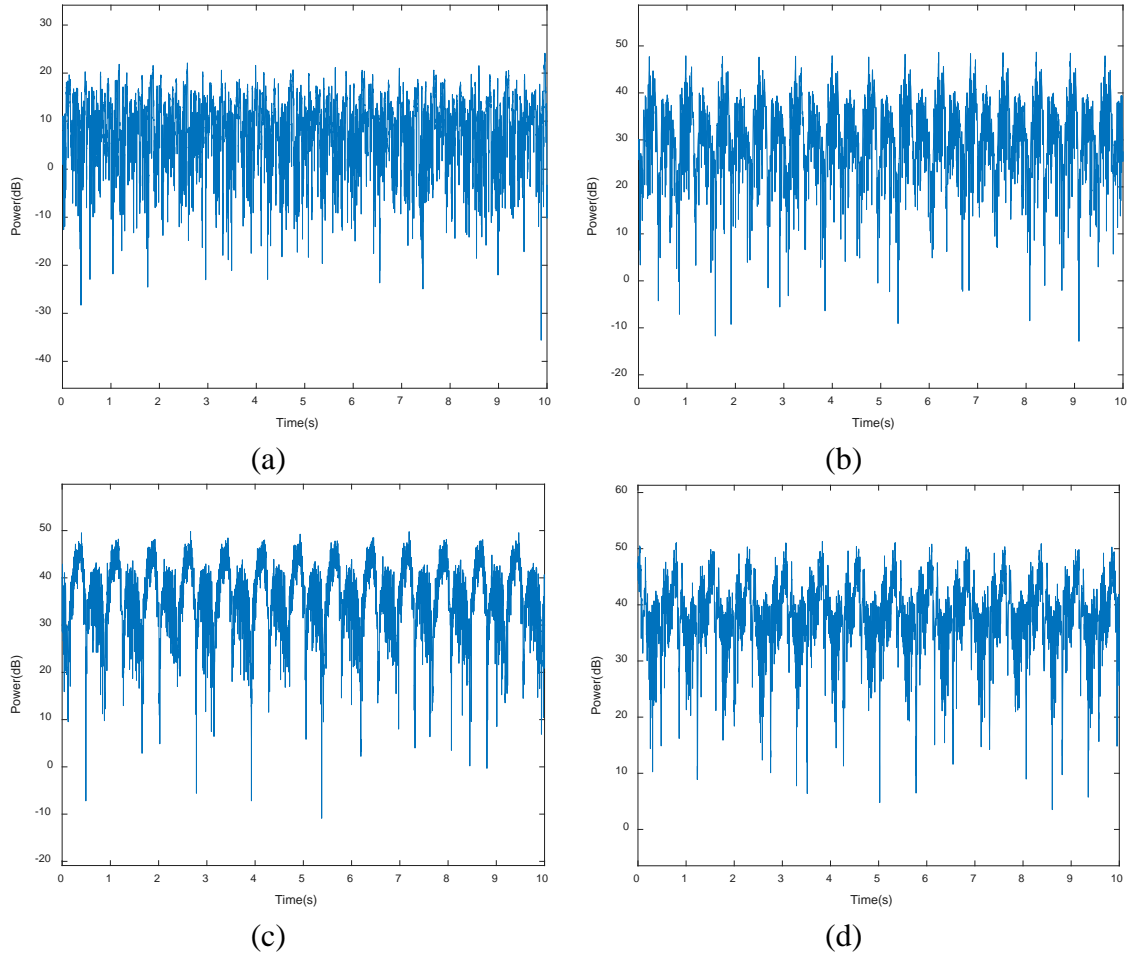
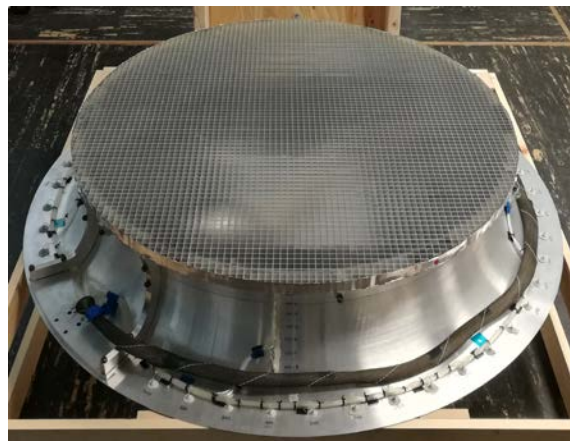


Figure 26. Power Plot for Antenna at (a) 0° , (b) 20° , (c) 40° , and (d) 60° Offset Angle from Rotator at 80 rpm

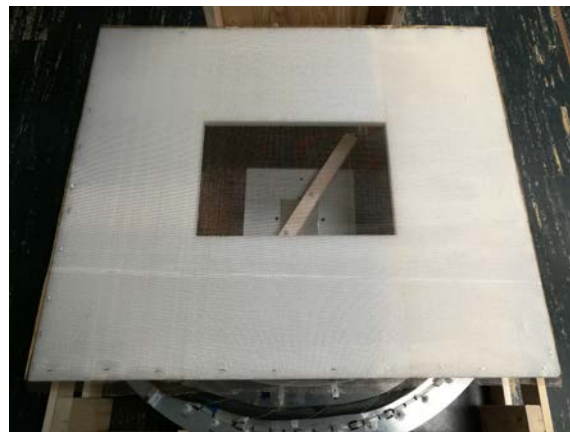
Next, we take measurements for the three configurations shown in Figure 27: (1) with shroud, (2) with shroud and screen, and (3) with shroud and wire mesh. The shroud is made of aluminum and is approximately 0.9 m in diameter at the front (narrow) opening. It is approximately a 1/10 scaled model of what would be used on a small commercial 20-kW WT with a rotor diameter of 10.0 m. A comparison of the data is given in Tables 4 through 7.



(a)



(b)



(c)

Figure 27. Different Configurations for Measurements: (a) Shroud, (b) Shroud and 0.5 Inch by 0.5 Inch Screen, and (c) Shroud and 1.0 mm by 1.0 mm Wire Mesh

At the 0° offset, the configuration with the shroud and screen gave the largest attenuation of approximately 20 dB, while the other two configurations gave an attenuation of approximately 12 dB, as shown in Table 4. The typical Doppler signature of the rotator was also not observed from the spectrogram.

At the 20° offset, the addition of the shroud does not cause much difference to the power level but appears to increase Doppler clutter. This can be due to the multibounce effect [12], where the reflected waves from the metallic ball are reflected from the shroud and floor before returning to the receiving antenna. We observed power attenuations of approximately 35 dB and 40 dB, shown in Table 5, with the addition of the screen and wire mesh, respectively.

At the 40° offset, similar to the result for 20° , the addition of the shroud does not cause much difference in the power level but appears to increase Doppler clutter due to the multibounce effect from the shroud and floor. We observed power attenuations of approximately 35 dB and 40 dB, shown in Table 6, with the addition of the screen and wire mesh, respectively.

At the 60° offset, similar to the previous result, the addition of the shroud does not cause much difference to the power level but appears to increase Doppler return due to multibounce from the shroud and floor. We observed power attenuation of approximately 30 dB, shown in Table 7, with the addition of the screen or wire mesh.

In summary, the addition of the shroud causes an increase in the Doppler return due to the multibounce effect, and an average reduction of about 30 dB in reflected power can be achieved with the addition of the screen or wire mesh. The measurement for the 0.5 inch by 0.5 inch screen agrees reasonably well with the 14 dB one-way attenuation from the simulated result, and approximately 18 dB one-way attenuation expected for the wire mesh.

Table 4. Spectrogram and Power Plot Comparison for Antenna at 0° Offset Angle for Different Cases for Rotator

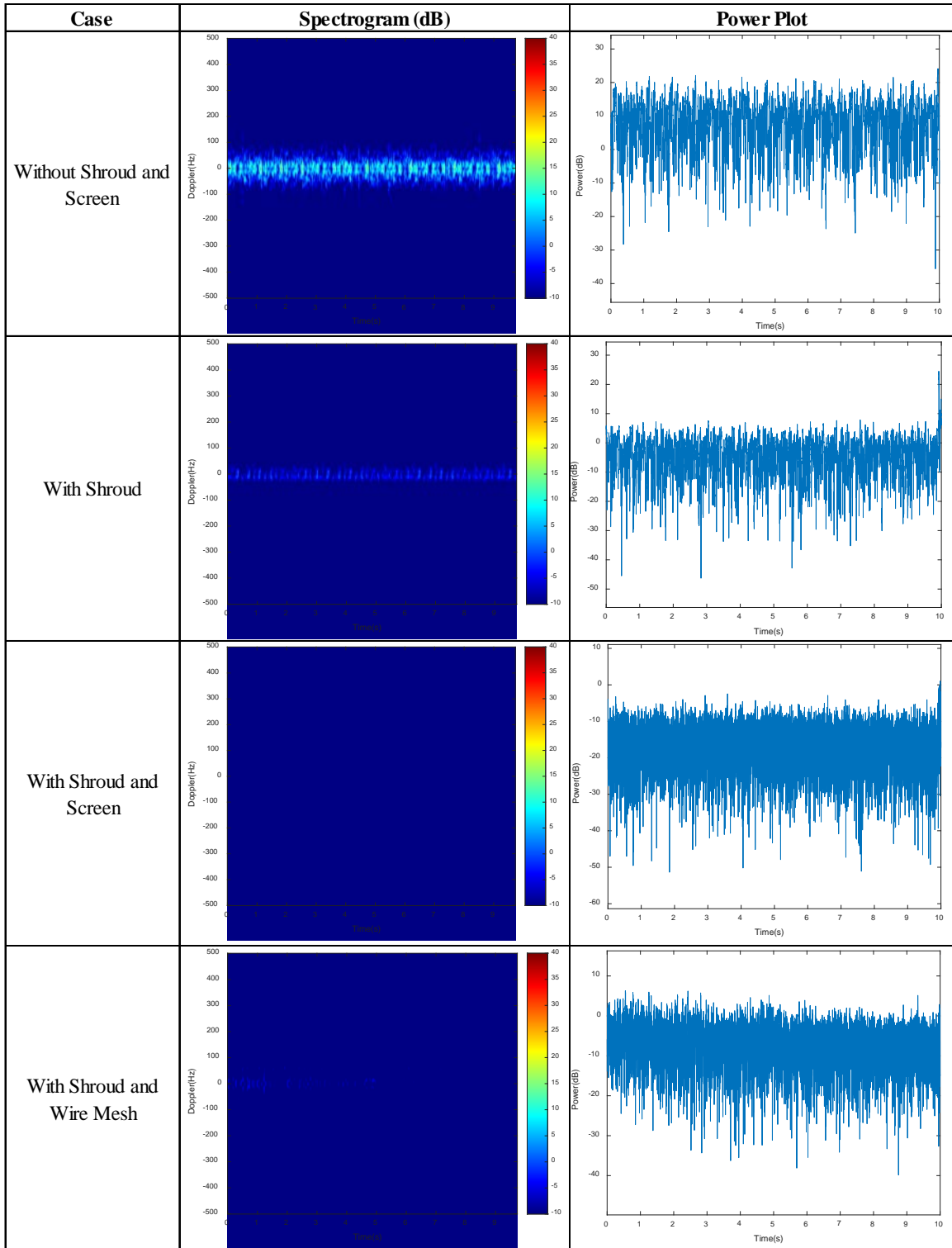


Table 5. Spectrogram and Power Plot Comparison for Antenna at 20° Offset Angle for Different Cases for Rotator

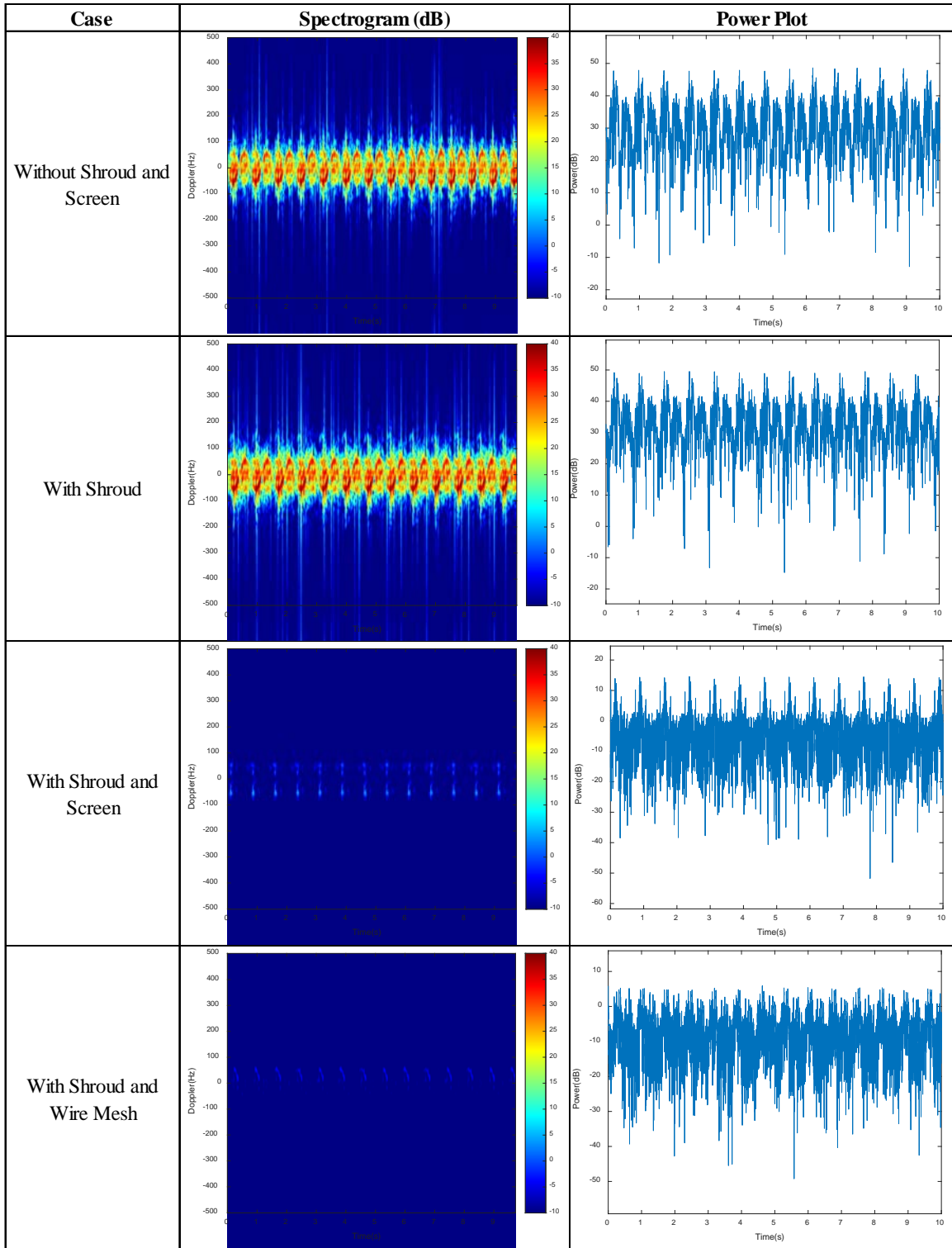


Table 6. Spectrogram and Power Plot Comparison for Antenna at 40° Offset Angle for Different Cases for Rotator

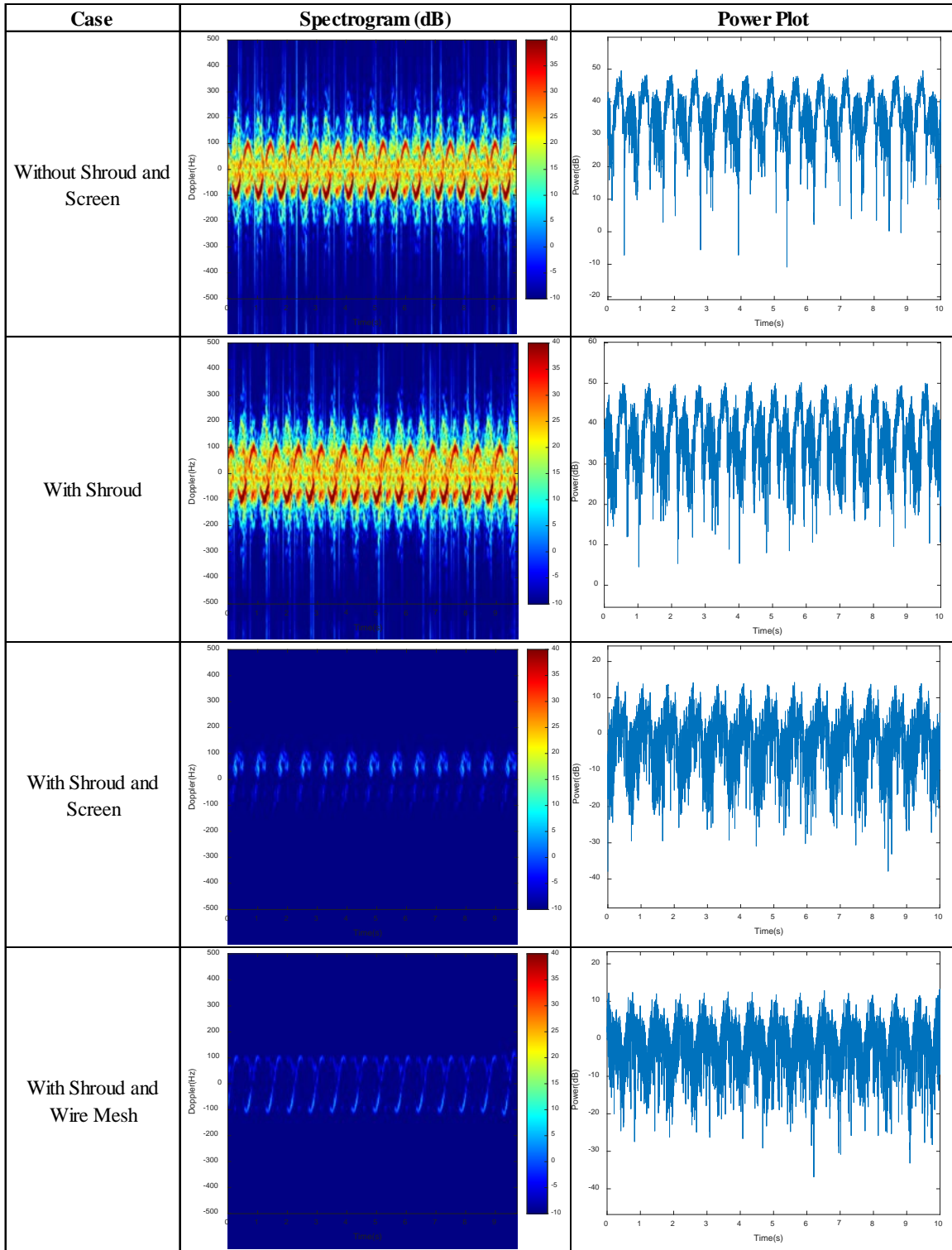
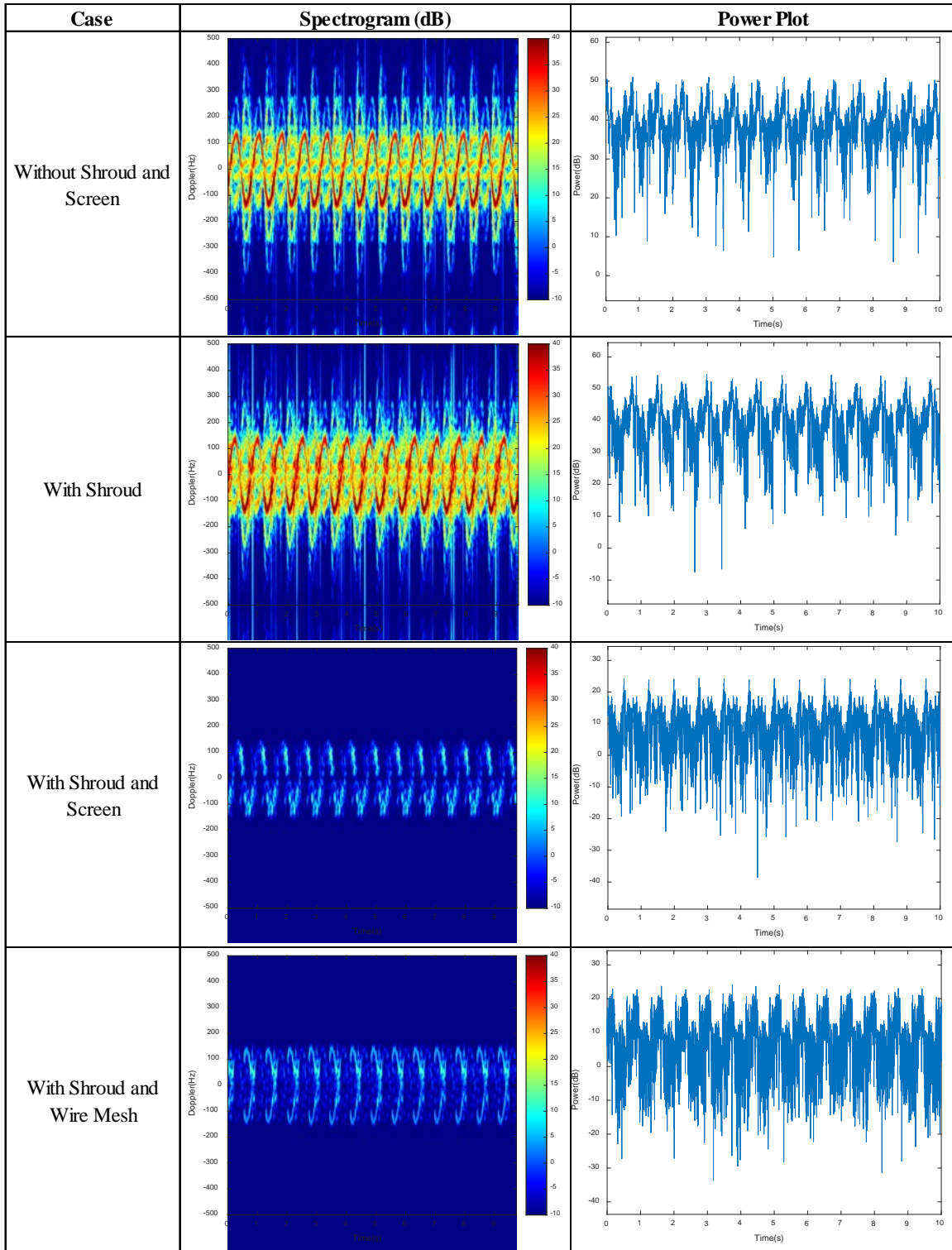


Table 7. Spectrogram and Power Plot Comparison for Antenna at 60° Offset Angle for Different Cases for Rotator



3. Measurement Results for the Wind Turbine Model

Measurements for the wind turbine model and fiberglass shroud were taken at Port Hueneme (Naval Facilities Engineering and Expeditionary Warfare Center–NAVFAC EXWC). The test setup is shown in Figure 28 and Figure 29. The three different configurations for measurement are shown in Figure 30. The distance between the wind turbine model and antenna is 12 ft (3.66 m). The wind turbine model is tilted in azimuth for the angle offset instead of tilting the radar antenna as in the rotator case. The wind turbine is also rotating at a faster speed of 120 rpm. Similarly, the shroud in use is larger than the one previously used with the rotator and is made of composite fiberglass with a thickness of about two inches. In addition, there is a vertical aluminum septum behind the rotor.

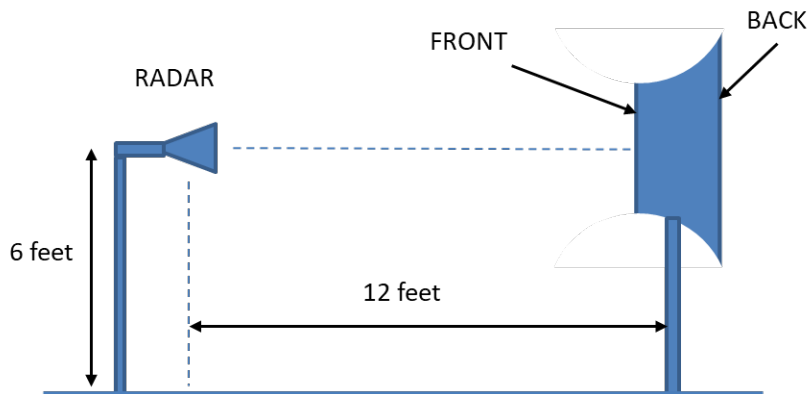


Figure 28. Side View of the Setup for Wind Turbine Measurement

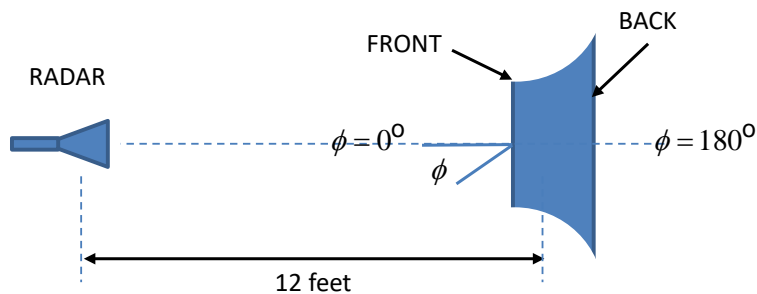


Figure 29. Top View of the Setup for Wind Turbine Measurement

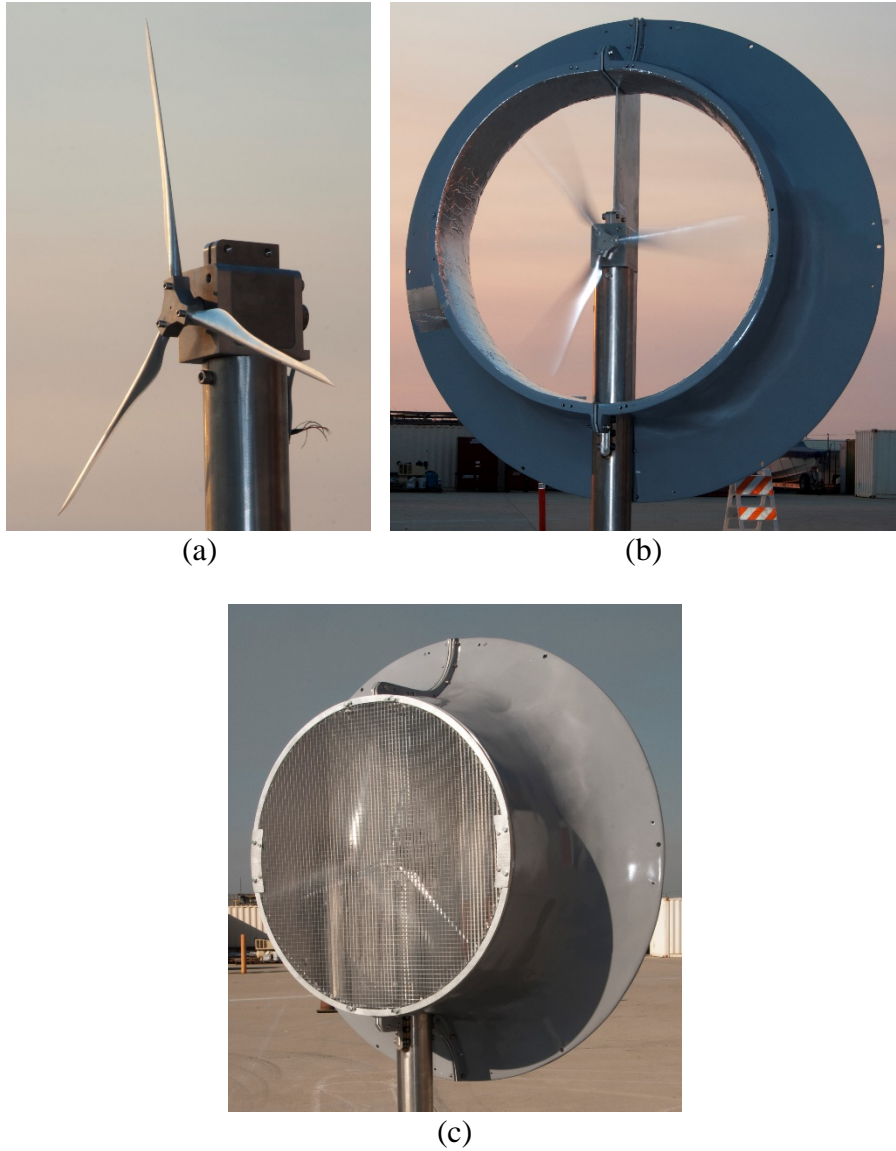


Figure 30. Wind Turbine Model Configurations: (a) Bare, (b) with Shroud, and (c) Shroud and 0.5 Inch by 0.5 Inch Screen

Measurements are conducted first on the bare configuration (just the wind turbine) to obtain the reference data for subsequent comparison. The wind turbine model rotates at 120 rpm, generating a maximum Doppler return of about 168 Hz, as shown in Figure 31. The data was collected for 10.0 s at 128 samples per sweep with a sweep time of 1.0 ms.

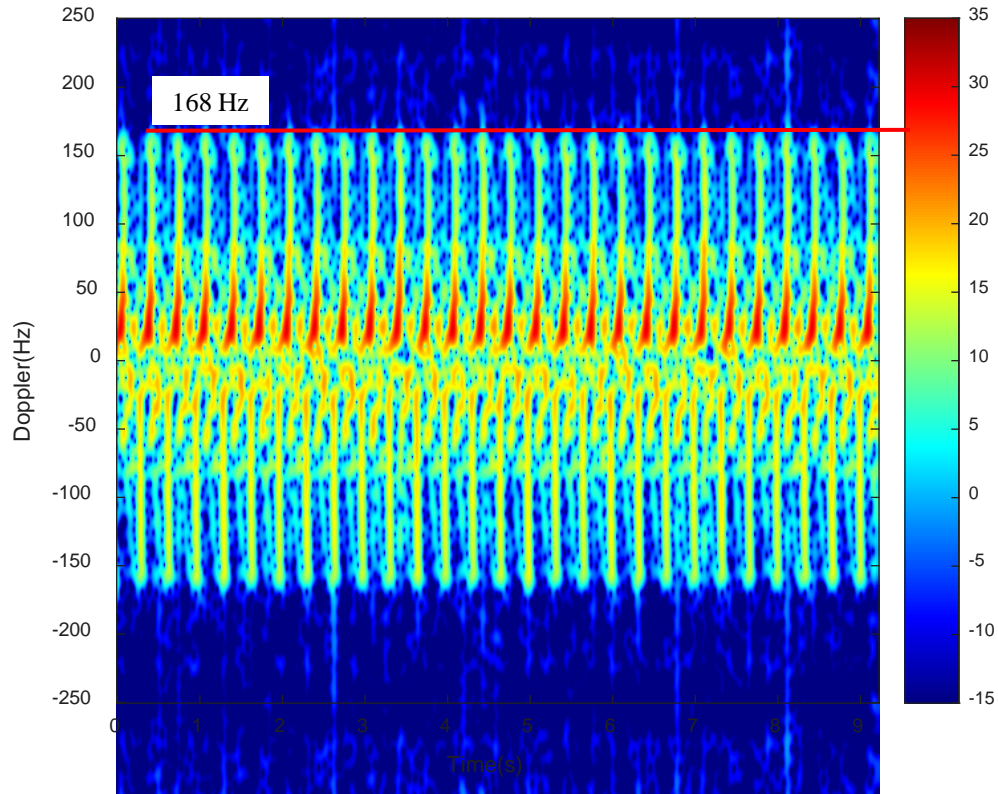


Figure 31. Doppler Spectrogram for Antenna at 90° Offset Angle from Wind Turbine Model at 120 rpm

From the spectrograms shown in Figure 32, the results are similar as compared to those for the rotator described in Section B.2. The Doppler return frequency increased as the offset angle increased to reach its maximum at 90°. At the 0° offset angle, some Doppler return was captured as is the case observed for the rotator and does not display the typical Doppler signature from wind turbine. This could be due to the alignment between the wind turbine and the antenna, and the hub's uneven surfaces at the center of the rotor could also have contributed to the Doppler return. The reflections from the blades off from the tower contributed to the Doppler return as well.

The Doppler signature from the wind turbine is significantly different from that of the rotator, displaying as a sharp spike instead of the sinusoidal shape from the rotator. The differences of the signature are mainly due to the design of the blade, which is thin and

long while the metallic ball is round. The Doppler return frequency is also higher, since the wind turbine is rotating at a higher rpm.

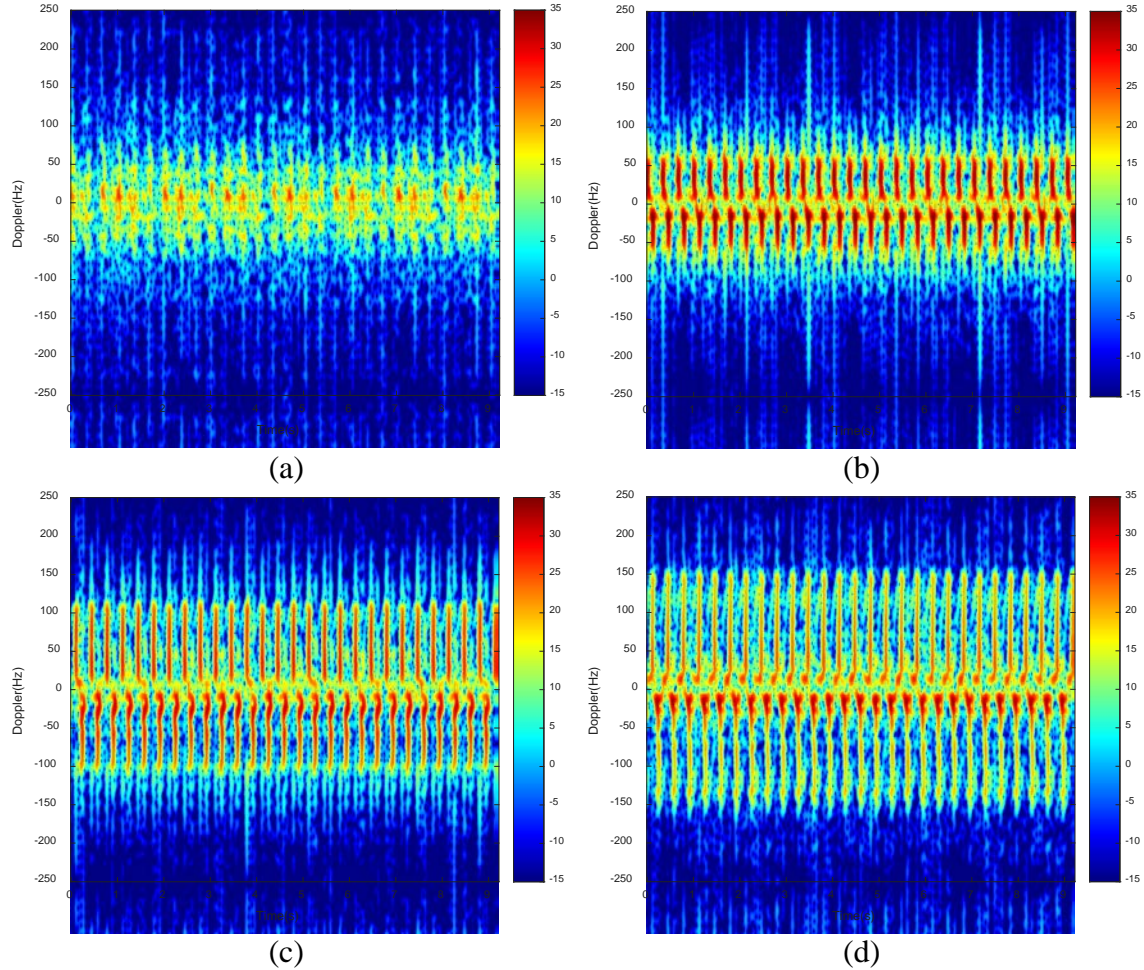


Figure 32. Doppler Spectrogram for Antenna at (a) 0° , (b) 20° , (c) 40° , and (d) 60° Offset Angle from Wind Turbine Model at 120 rpm

The expected Doppler characteristics based on the measured maximum Doppler agree reasonably well with the measured Doppler for most of the angles, as seen from Table 8 and Figure 33, except in the region between 0° to 10° , where the factors that may have contributed to the differences between the expected and measured Doppler return frequencies were discussed earlier.

Table 8. Comparison between Theoretical and Measured Doppler Return Frequency for Wind Turbine Model

Offset (°)	Expected Doppler (Based on $f_{Dmax} = 168$ Hz)	Measured Doppler (Hz)
0	0	23
10	29.2	41
20	57.5	58
30	84	89
40	108.0	110
50	128.7	127
60	145.5	145

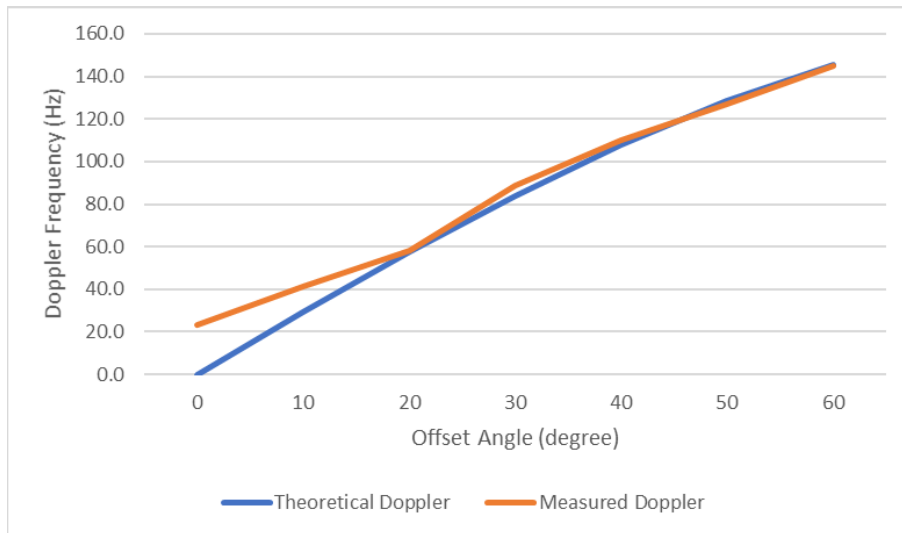


Figure 33. Comparison between Theoretical Doppler and Measured Doppler Frequencies for Wind Turbine Model

The power of the received signal at different antenna offset angles was processed, and the peak power of the envelope was compared, as shown in Figure 34. Besides the case when the antenna is at 0° offset angle at about 30 dB, the power falls between 42 dB to 45 dB. The results in Figures 32 and 34 serve as the baseline for comparison with the other two measurement configurations.

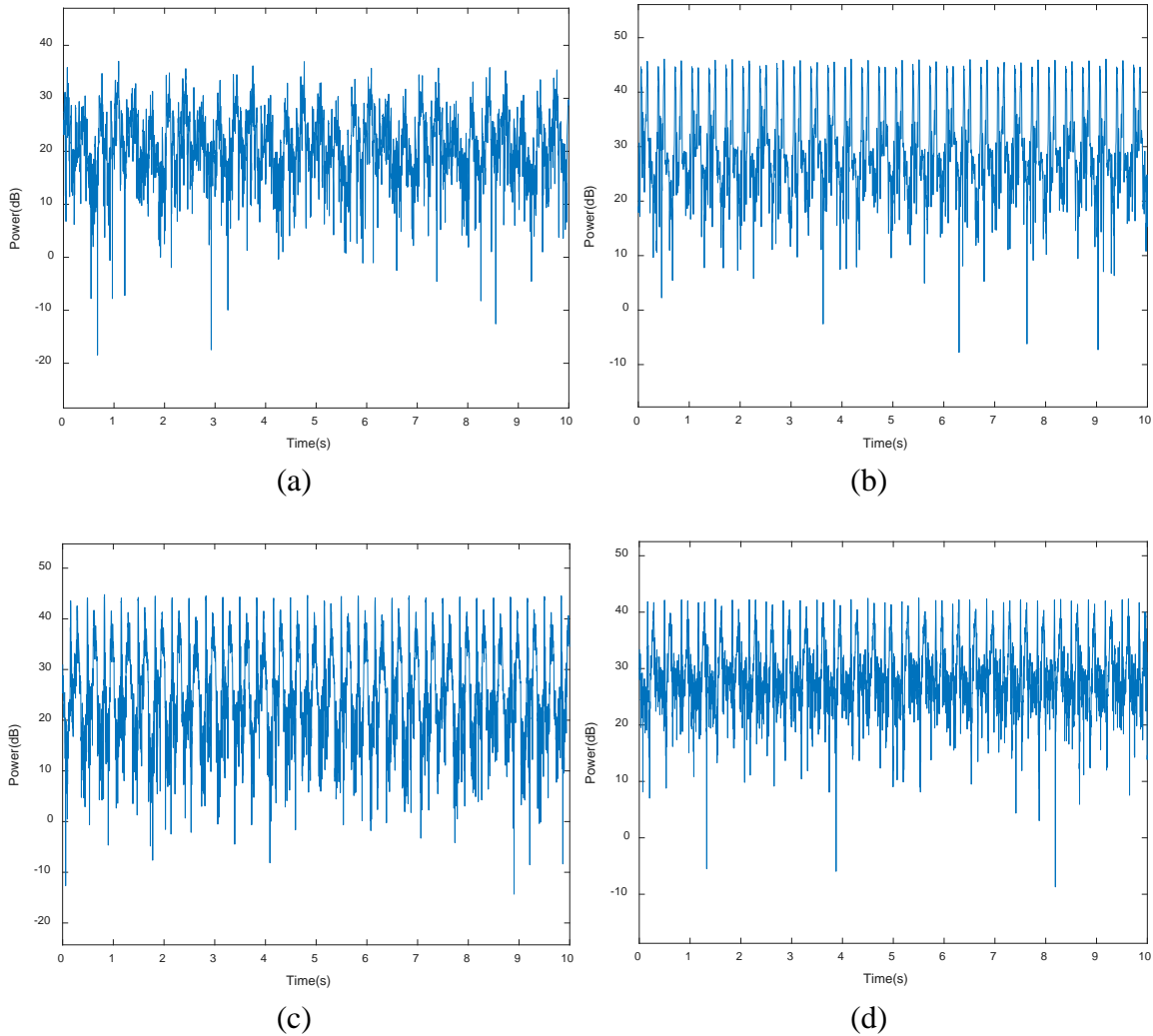


Figure 34. Power Plot for Antenna at (a) 0° , (b) 20° , (c) 40° , and (d) 60° Offset Angle from Wind Turbine Model at 120 rpm

The results for different configurations at different offset angles were compared and are shown in Tables 9 to 12. At the 0° offset angle, there is power attenuation of about 20 dB for the shroud configuration and attenuation of about 25 dB for the shroud and screen configuration. Most of the Doppler return was suppressed, and this is more evident in the spectrogram of the shroud and screen configuration.

At the 20° offset angle, there is no significant difference between the power levels of the bare configuration and the shroud and screen configuration. The power level remained at about 45 dB; although, the shroud configuration power level was about

2–3 dB larger. This could be due to the aluminum septum of the shroud that becomes more visible as the angle increases. In addition, there is also transmission through the shroud (which is made of fiberglass), which adds on to the return power. With the addition of the 0.5 inch by 0.5 inch screen in front of the wind turbine, the power level was attenuated by about 25 dB, reducing the Doppler return as well. The wind turbine Doppler signature remains observable but at a reduced strength of about 10 dB on the spectrogram.

At the 40° offset angle, power levels for both the bare and shroud configurations remain about the same at about 42 dB. As in previous case, the Doppler return increases due to the shroud. Power attenuation of about 22 dB was achieved with the addition of the screen. The wind turbine Doppler signature remains observable at about 10 dB on the spectrogram.

At the 60° offset angle, power levels for both the bare and shroud configurations remain about the same at about 42 dB. We also observe increased Doppler returns due to the shroud. Power attenuation of about 30 dB was achieved with the screen. The higher attenuation is likely due to the shroud and screen obscuring the view of the antenna on the wind turbine. The scattering effects from the screen and curvature of the shroud contributed to the weaker returns back to the antenna as well. Traces of the wind turbine Doppler signature can still be observed at about 5 dB on the spectrogram.

In summary, the addition of the shroud causes an increase in the Doppler return due to the multibounce effect from non-metallic shroud, which permits most of the transmission to pass through with slight attenuation. An average reduction of about 25 dB in reflected power can be achieved with the addition of the 0.5 inch by 0.5 inch screen with the shroud.

Table 9. Spectrogram and Power Plot Comparison for Antenna at 0° Offset Angle for Different Cases for Wind Turbine Model

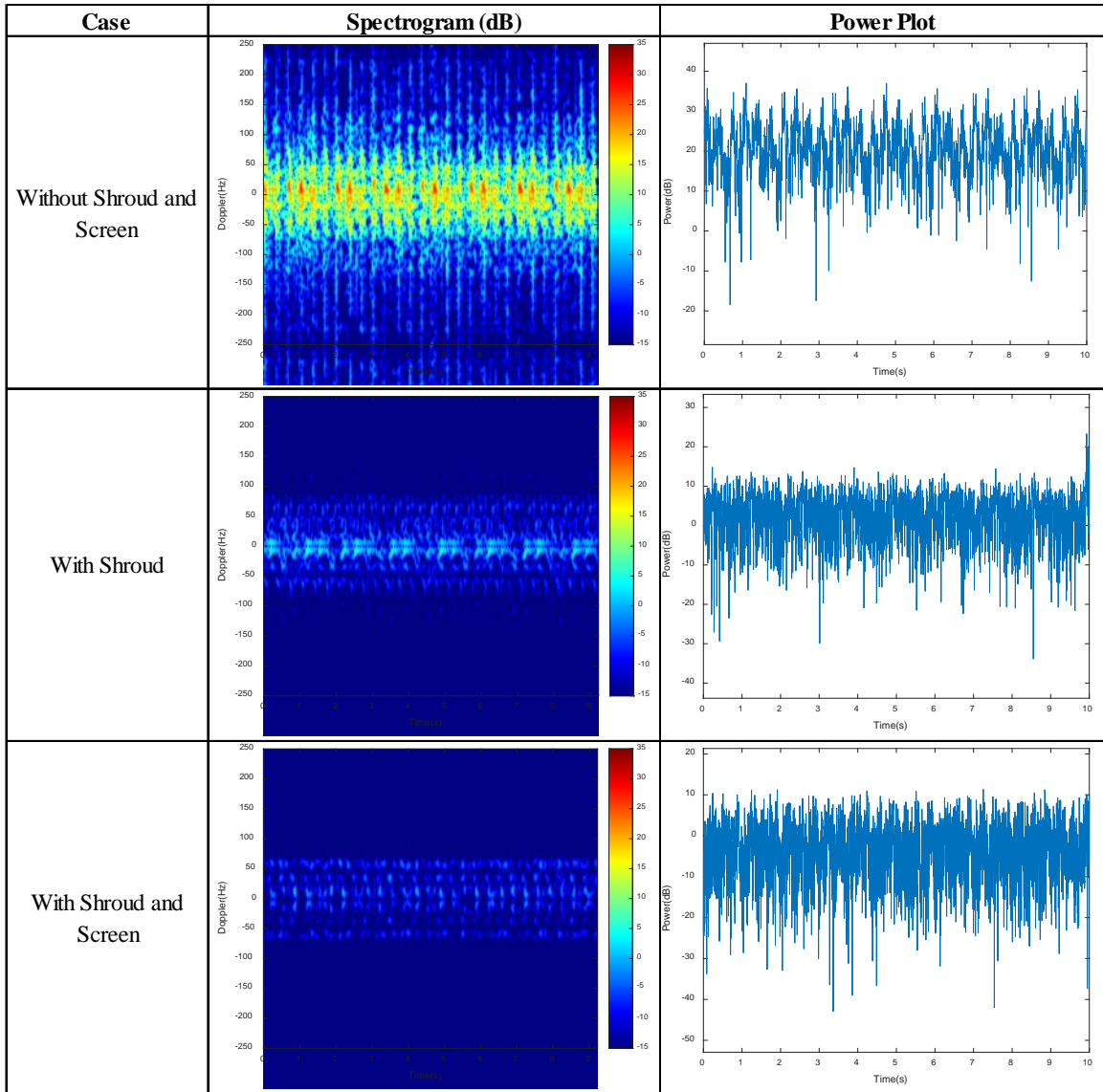


Table 10. Spectrogram and Power Plot Comparison for Antenna at 20° Offset Angle for Different Cases for Wind Turbine Model

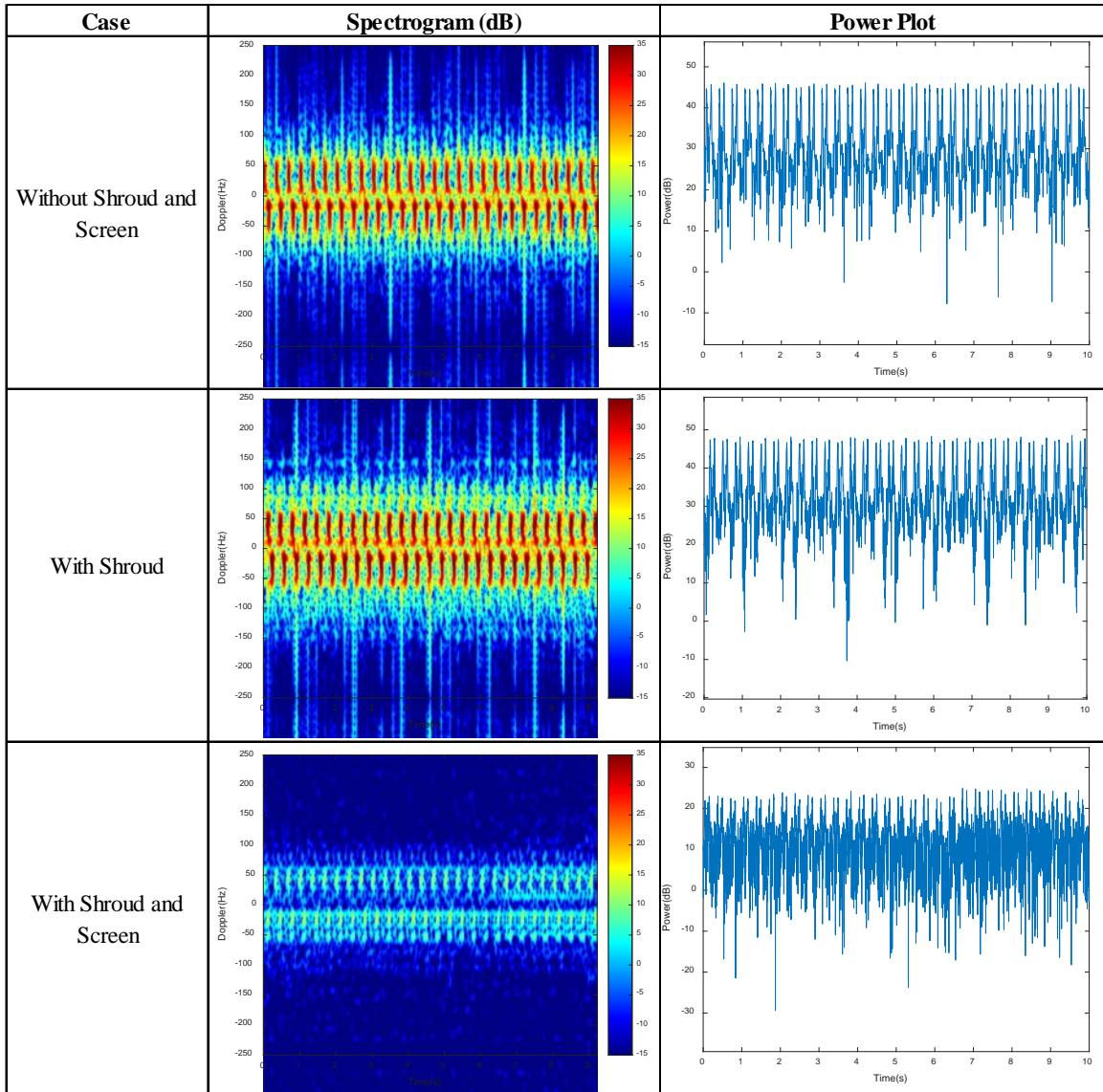


Table 11. Spectrogram and Power Plot Comparison for Antenna at 40° Offset Angle for Different Cases for Wind Turbine Model

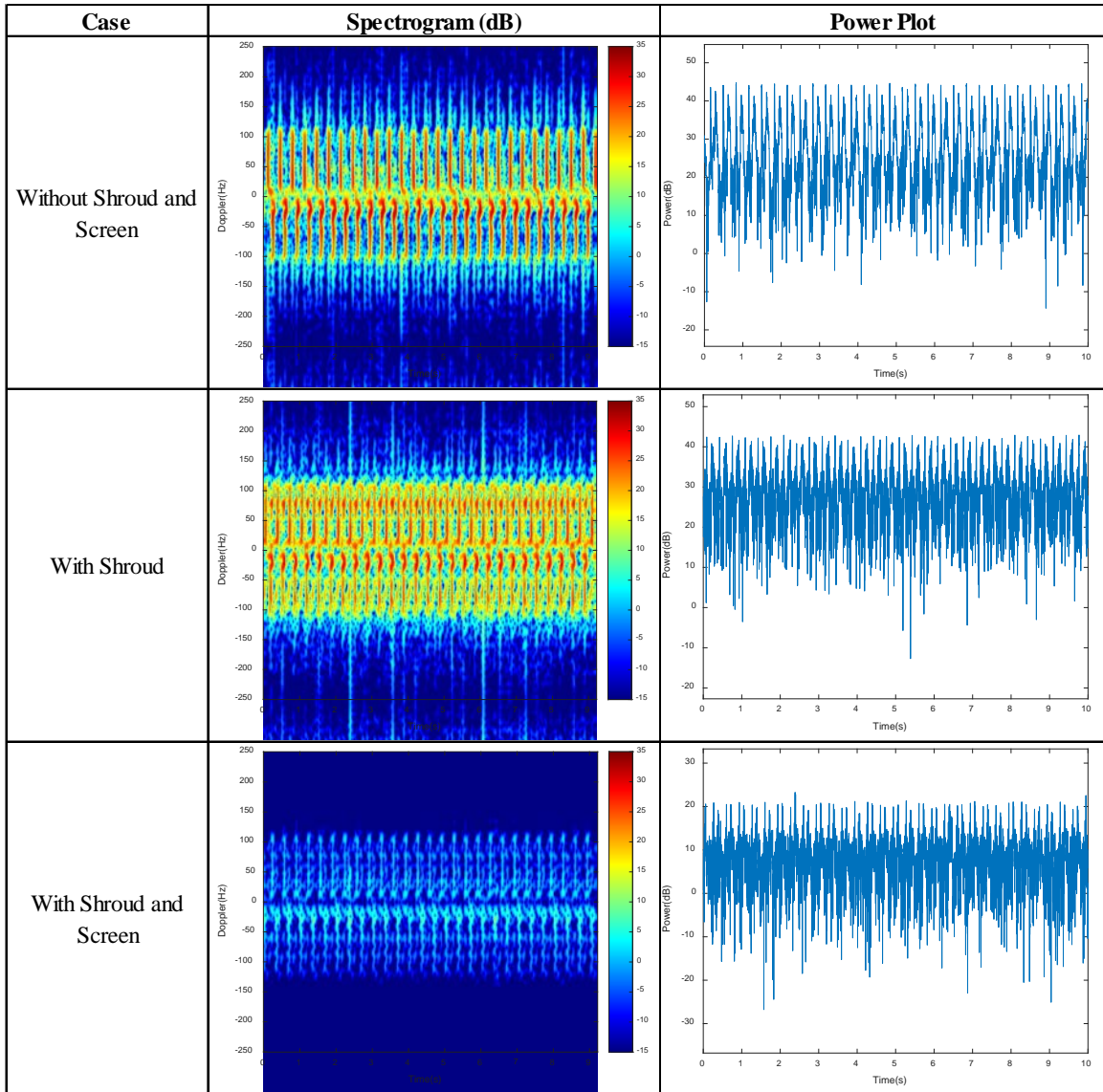
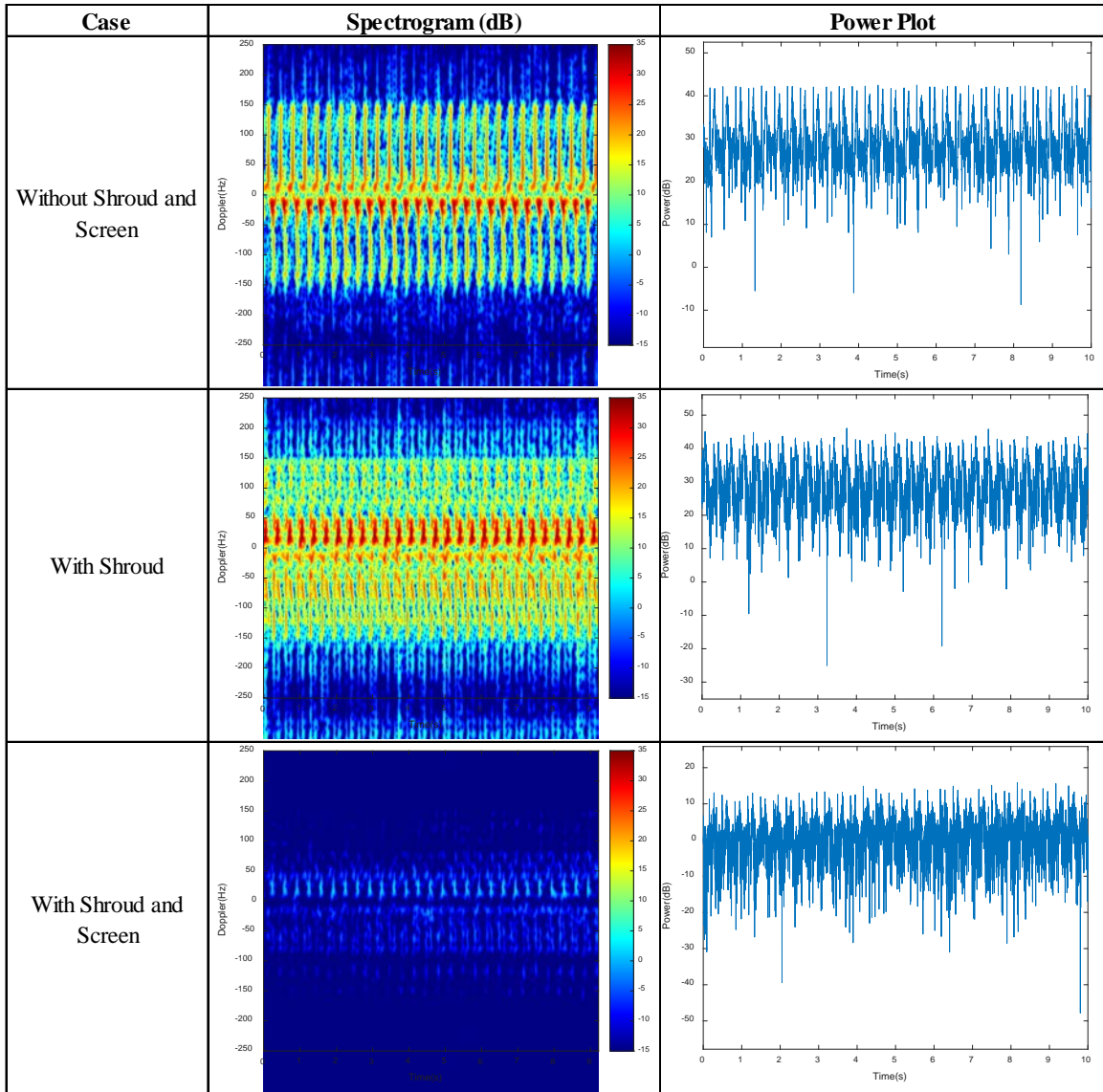


Table 12. Spectrogram and Power Plot Comparison for Antenna at 60° Offset Angle for Different Cases for Wind Turbine Model



In this chapter, simulation results on the reduction effect of the screens were shown and compared to the measurement results. The measurement setup and procedure were also presented. Measurement results in the form of spectrograms and power plots for both the rotator and wind turbine model at various offset angles were compared for analysis of the screens' effectiveness in reducing the Doppler interference from the rotator and wind turbine blades.

The summary of findings and recommendations for future work are presented in the next chapter.

THIS PAGE INTENTIONALLY LEFT BLANK

IV. SUMMARY AND CONCLUSIONS

A. SUMMARY OF FINDINGS

In this thesis, we investigated the effectiveness of the addition of a shroud and screen to the wind turbine to reduce Doppler interference to radar system. The addition of a shroud enhances the air flow rate through the wind turbine, and the screen and shroud can act as a reflector of electromagnetic waves before reaching the wind turbine blades. The addition of the shroud and screen can potentially increase the static RCS of the wind turbine, but most radar processors are able to detect and track moving targets-of-interest using the filtering techniques mentioned in Chapter I.

The software-defined radar employed in this research, SDR-KIT 980AD, is suitable for use in the laboratory due to its compact size. It is also able to provide the raw I and Q data for post-processing to extract the Doppler returns for analysis. The capabilities of the SDR were first verified using the rotator built in the control laboratory before measurements were carried out with the shroud and screen. Finally, we performed measurements on a 1/10 scale model of a WT with and without the shroud and screen.

1. Findings for Rotator

The addition of a shroud made of aluminum, which is reflective in nature, increases Doppler return back to the radar except in the case of the 0° offset angle where the Doppler return was attenuated. This could be due to the reflection from the floor behind the rotator where destructive interference can occur. There are also contributions due to reflections from the internal surface of the shroud. At other offset angles, an average power level increase of approximately 1 to 3 dB was observed, likely due to the multipath from the internal surface of the shroud. With the inclusion of the screen (0.5 inch by 0.5 inch openings) or wire mesh (1.0 mm by 1.0 mm openings), we observed a power level attenuation of at least 30 dB. The performance of the 0.5 inch by 0.5 inch screen and the wire mesh is comparable. As such, the screen is a better choice for application as the coarser the weave, the less effect the screen has on air flow to the wind turbine.

2. Findings for Wind Shroud Model

Similar results were observed from the measurement for the wind shroud model; although, the design and material used for the shroud are slightly different compared to those used for the rotator. The fiberglass shroud only provides about 4 to 5 dB of two-way loss (based on a relative dielectric constant $\epsilon_r = 4.2$, loss tangent $\tan \delta = 0.015$, and 2.0 inch thickness). We observed increased Doppler return when the antenna was offset from the wind turbine except in the case of the 0° offset. We also observed an average power level attenuation of 25 dB when a 0.5 inch by 0.5 inch screen was placed before the wind turbine, which is comparable to the result for the rotator measurement.

From the measurements, it was verified that with the usage of a screen with 0.5 inch by 0.5 inch openings and the shroud, the Doppler return can be reduced by at least 25 dB, potentially mitigating the Doppler interference to the radar system. A metal shroud with a common window screen (or finer mesh) is more effective than a shroud alone. Mesh attenuation is only marginally better than screen. Although this study focuses on a single wind turbine, the basis for further research into large-scale implementation has been established.

B. FUTURE WORK

Future work to reduce Doppler interference can be done in a few ways. First, the usage of RAM on the shroud can be explored to further reduce the Doppler return from rotor reflections from the shroud. Simulation using ray-tracing methods can be employed to understand the reflected wave trajectories within the shroud for the development of other Doppler reduction approaches. Furthermore, different geometric designs of the screen weave can be explored to further reduce the Doppler interference to radar system while maintaining the wind flow rate for maximum wind turbine efficiency. Lastly, simulation can be carried out to understand the effectiveness of shroud and screen in reducing Doppler interference from wind turbine in large-scale implementation in order to determine the viability of this approach.

LIST OF REFERENCES

- [1] IPCC. “Climate change 2014: Synthesis report,” Geneva, Switzerland, 2014. [Online]. Available: http://www.ipcc.ch/pdf/assessment_report/ar5/syr/SYR_AR5_FINAL_full_wcover.pdf
- [2] “History of U.S. wind energy,” Office of Energy Efficiency & Renewable Energy. Accessed Oct. 9, 2017. [Online]. Available: <https://energy.gov/eere/wind/history-us-wind-energy>
- [3] “Wind energy facts at a glance,” American Wind Energy Association. Accessed Oct. 9, 2017. [Online]. Available: <https://www.awea.org/wind-energy-facts-at-a-glance>
- [4] Office of the Director of Defense Research and Engineering, “The effect of windmill farms on military readiness,” Report to Congressional Defense Committees, Washington, DC, USA, 2006. [Online]. Available: <http://www.dtic.mil/dtic/tr/fulltext/u2/a455993.pdf>
- [5] M. Kavinsky, “Wind farm interference shows up on Doppler radar,” National Weather Service. Accessed Oct. 20, 2017. [Online]. Available: <https://www.weather.gov/mkx/windfarm>
- [6] C. A. Jackson and M. M. Butler, “Options for mitigation of the effects of windfarms on radar systems,” in *IET Int. Conf. Radar Sys.*, 2007, pp. 1–6.
- [7] J. Pinto, J. C. G. Matthews, and G. C. Sarno, “Stealth technology for wind turbines,” in *IET Radar, Sonar & Navigation*, vol. 4, no. 1, pp. 126–133, Feb. 2010. [Online]. doi: 10.1049/iet-rsn.2009.0031
- [8] J. P. Scheuermann, “Wind flow through shrouded wind turbines,” M.S. thesis, Dept. of Mech. and Aeros. Eng., NPS, Monterey, CA, USA, 2017. [Online]. Available: <http://hdl.handle.net/10945/53045>
- [9] D. Jenn, *Radar and Laser Cross Section*, 2nd ed., Reston, VA, USA: AIAA Education Series, 2005.
- [10] A. Balleri, A. Al-Armaghany, H. Griffiths, K. Tong, T. Matsuura, T. Karasudani, Y. Ohya, “Measurements and analysis of the radar signature of a new wind turbine design at X-band,” in *IET Radar, Sonar & Navigation*, vol. 7, no. 2, pp. 170–177, Feb. 2013. [Online]. doi: 10.1049/iet-rsn.2012.0026
- [11] A. Naqvi, S. T. Yang, and H. Ling, “Investigation of Doppler features from wind turbine scattering,” in *IEEE Antennas and Wireless Propagation Letters*, vol. 9, pp. 485–488, 2010. [Online]. doi: 10.1109/LAWP.2010.2050672

- [12] V. C. Chen, *The Micro-Doppler Effect in Radar*. Boston, MA, USA: Artech House, 2011.
- [13] M. I. Skolnik, *Introduction to Radar Systems*, 3rd ed., New York, NY, USA: McGraw-Hill, 2001.
- [14] D. Vegas, J. C. G. Matthews, L. Norin, and I. Angulo, "Mitigation techniques to reduce the impact of wind turbines on radar services," *Energies* 2013, vol. 6, no. 6, pp. 2859–2873, Jun. 2013. [Online]. doi:10.3390/en6062859
- [15] T. Debatty, "Software defined RADAR, a state of art," *2nd International Workshop on Cognitive Information Processing*, 2010, pp. 253–257. [Online]. doi: 10.1109/CIP.2010.5604241
- [16] Ancortek, "User manual. Rev 1.3," Fairfax, VA, USA: Ancortek Inc., 2016.
- [17] B. Liu and R. Chen, "Software-defined radar and waveforms for studying micro-Doppler signatures," in *Proc. SPIE 9077, Radar Sensor Technology XVIII*, 907718, May 29, 2014. [Online]. doi: 10.1117/12.2051044
- [18] "WR-90 Waveguide standard gain horn antenna operating from 8.2 GHz to 12.4 GHz with a nominal 20 dB gain SMA female input," Pasternack. Accessed Jan. 14, 2018. [Online]. Available: <https://www.pasternack.com/images/ProductPDF/PE9856-SF-20.pdf>
- [19] C. Roberto, *Modern Digital Signal Processing*. Pacific Grove, CA, USA: Thomson/Brooks/Cole, 2004.
- [20] "Introduction to I&Q imbalance correction," Ancortek, Inc. Accessed Jan. 13, 2018. [Online]. Available: <http://ancortek.com/micro-doppler-analysis-iq-imbalance-correction>
- [21] Keysight Technologies, "8496H programmable step attenuator, DC to 18 GHz, 0 to 110 dB, 10 dB steps," Aug. 2014. [Online]. Available: <https://www.keysight.com/main/redirector.jsp?action=ref&cname=EDITORIAL&cckey=1763127&lc=eng&cc=US&nfr=-32726.536879906.00>
- [22] W. Stutzman and G. Thiele, *Antenna Theory and Design*, 3rd ed., Hoboken, NJ, USA: Wiley, 2013.

INITIAL DISTRIBUTION LIST

1. Defense Technical Information Center
Ft. Belvoir, Virginia
2. Dudley Knox Library
Naval Postgraduate School
Monterey, California